Contrib Mineral Petrol (1990) 104:99–124

Contributions to Mineralogy and Petrology

H, O, Sr, Nd, and Pb isotope geochemistry of the Latir volcanic field and cogenetic intrusions, New Mexico, and relations between evolution of a continental magmatic center and modifications of the lithosphere

Clark M. Johnson[1], **Peter W. Lipman**[2], **and Gerald K. Czamanske**[3]

[1] Department of Geology and Geophysics, University of Wisconsin, Madison, WI 53706, USA
[2] US Geological Survey, Mail Stop 903, Denver, CO 80225, USA
[3] US Geological Survey, Mail Stop 984, Menlo Park, CA 94025, USA

Abstract. Over 200 H, O, Sr, Nd, and Pb isotope analyses, in addition to geologic and petrologic constraints, document the magmatic evolution of the 28.5–19 Ma Latir volcanic field and associated intrusive rocks, which includes multiple stages of crustal assimilation, magma mixing, protracted crystallization, and open- and closed-system evolution in the upper crust. In contrast to data from younger volcanic centers in northern New Mexico, relatively low and restricted primary $\delta^{18}O$ values (+6.4 to +7.4) rule out assimilation of supracrustal rocks enriched in ^{18}O. Initial $^{87}Sr/^{86}Sr$ ratios (0.705 to 0.708), ε_{Nd} values (−2 to −7), and $^{206}Pb/^{204}Pb$ ratios (17.5 to 18.4) of metaluminous precaldera volcanic rocks and postcaldera plutonic rocks suggest that most Latir rocks were generated by fractional crystallization of substantial volumes of mantle-derived basaltic magma that had near-chondritic Nd isotope ratios, accompanied by assimilation of crustal material in two main stages: 1) assimilation of non-radiogenic lower crust, followed by 2) assimilation of middle and upper crust by intermediate-composition magmas that had been contaminated during the first stage. Magmatic evolution in the upper crust peaked with eruption of the peralkaline Amalia Tuff (~26 Ma), which evolved from metaluminous parental magmas. A third stage of late, roofward assimilation of Proterozoic rocks in the Amalia Tuff magma is indicated by trends in initial $^{87}Sr/^{86}Sr$ and $^{206}Pb/^{204}Pb$ ratios from 0.7057 to 0.7098 and 19.5 to 18.8, respectively, toward the top of the pre-eruptive magma chamber. Highly evolved postcaldera plutons are generally fine grained and are zoned in initial $^{87}Sr/^{86}Sr$ and $^{206}Pb/^{204}Pb$ ratios, varying from 0.705 to 0.709 and 17.8 to 18.6, respectively. In contrast, the coarser-grained Cabresto Lake (~25 Ma) and Rio Hondo (~21 Ma) plutons have relatively homogeneous initial $^{87}Sr/^{86}Sr$ and $^{206}Pb/^{204}Pb$ ratios of approximately 0.7053 and 17.94 and 17.55, respectively. ε_{Nd} values for all the postcaldera plutons overlap those of the precaldera rocks and Amalia Tuff, except for those for two late-stage rhyolite dikes associated with the Rio Hondo pluton that have ε_{Nd} values of −8.6 and −9.5; these dikes are the only Latir rocks which may be largely crustal melts.

Chemical and isotopic data from the Latir field suggest that large fluxes of mantle-derived basaltic magma are necessary for developing and sustaining large-volume volcanic centers. Development of a detailed model suggests that 6–15 km of new crust may have been added beneath the volcanic center; such an addition may result in significant changes in the chemical and Sr and Nd isotopic compositions of the crust, although Pb isotope ratios will remain relatively unchanged. If accompanied by assimilation, crystallization of pooled basaltic magma near the MOHO may produce substantial cumulates beneath the MOHO that generate large changes in the isotopic composition of the upper mantle. The Latir field may be similar to other large-volume, long-lived intracratonal volcanic fields that fundamentally owe their origins to extensive injection of basaltic magma into the lower parts of their magmatic systems. Such fields may overlie areas of significant crustal growth and hybridization.

Offprint requests to: C.M. Johnson

Introduction

Detailed petrologic studies of continental volcanic centers during the last decade have led to models for magmatic systems that involve varying rates of injection of mantle-derived basaltic magma into the crust, partial melting and fractionation, and extrusion of the resulting differentiated magmas (Smith 1979; Hildreth 1981; Shaw 1985). Three types of volcanic center may be distinguished (e.g., Shaw 1985): 1) small basalt-rhyolite fields associated with spatially restricted basaltic magma injection at low rates (e.g., Coso, California; Bacon 1982); 2) flood basalts associated with regional basaltic magma injection at high rates; and 3) large-volume intermediate- to silicic-composition volcanic centers, commonly associated with calderas (Lipman 1984), that represent crustal magmatism that is intermediate in terms of basaltic magma fluxes and extension to the first two types. At such caldera centers, injection rates for basaltic magma are sufficient to generate and sustain large, long-lived magmatic systems, in which prolonged crustal residence times allow generation of large volumes of compositionally zoned, generally crystal-poor silicic magma by various mechanisms. We will argue below that large fluxes of mantle-derived basaltic magma are needed to generate and sustain large silicic volcanic centers, and that the majority of rocks in the Latir field evolved by crystal fractionation of basaltic magma, accompanied by extensive interaction with the crust. This hypothesis is at odds with models that incorporate only minor basaltic components in the generation of silicic magmas by crustal melting (e.g., Chappell et al. 1987; Chappell and Stephens 1988).

Regional tilting and dissection by the Rio Grande rift has exposed an exceptional cross section through the late-Oligocene to early-Miocene Latir volcanic field and associated Questa caldera and cogenetic plutonic rocks in northern New Mexico (Fig. 1). Precaldera and caldera-related volcanic rocks evolved in an open system by crystal fractionation, magma mixing, and crustal assimilation (Johnson and Lipman 1988). In contrast, internal chemical and mineral variations within postcaldera plutonic rocks were generated largely by closed-system crystal fractionation of intermediate-composition parental magmas (Johnson et al. 1989). Granites were produced at the upper margins of crystal-rich chambers, largely by filter-pressing evolved magmas from crystal-rich "cumulate" zones. The plutonic suite represents the later stages of evolution of earlier high-level, subvolcanic magma chambers that were crystal poor.

Interpretation of the isotopic data presented here relies on previous geologic, petrologic, and geophysical work (Lipman 1983; Cordell et al. 1986; Hagstrum and Lipman 1986; Lipman et al. 1986; Dillet and Czamanske 1987; Czamanske and Dillet 1988; Johnson and Lipman 1988; Johnson et al. 1989; Lipman 1988; Lipman and Reed 1989). We develop here an integrated model for the origin and evolution of the Latir field, based on over 200 H, O, Sr, Nd, and Pb isotopic analyses, which we feel has general application to many caldera complexes. Our initial focus is on the origin of crustal components in the Latir magmas and their relations to evolution of the magmatic system. Discussion of the origin of large mantle components in the Latir rocks, identified largely by Nd isotope data, is centered on assimilation/fractional crystallization of basaltic magma versus melting of precursor basalts as possible models. We conclude with a semi-quantitative model for the effects of magmatism on the chemical and isotopic compositions of the pre-existing crust, young hybridized crust, and upper lithospheric mantle.

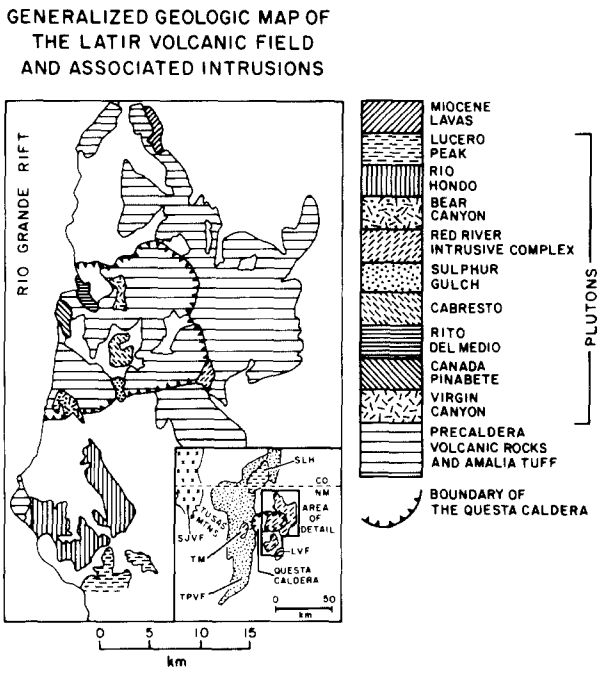

Fig. 1. Generalized geologic map of the Latir volcanic field and the Questa caldera exposed in the Sangre de Cristo Mountains of northern New Mexico, emphasizing the postcaldera intrusive rocks. *LVR* Latir volcanic field and associated intrusions; *TM* Timber and Brushy Mountains; *SJVF* San Juan volcanic field; *SLH* San Luis Hills; *TPVF* Taos Plateau volcanic field. The Rio Grande rift depression is largely delinated by the Taos Plateau volcanic field. Tusas Mountains lavas are temporally correlative with the Miocene lavas discussed here. San Luis Hills lavas are temporally correlative with caldera-related Latir rocks. Based on mapping by Lipman and Reed (1989)

Geologic setting

Erosional remnants of the Latir volcanic field cover an area of 1,200 km^2, and mark the southern part of an extensive composite Tertiary volcanic field exposed in the southern Rocky Mountains of southern Colorado and northern New Mexico (Steven 1975; Figs. 1 and 2). Most precaldera volcanic rocks (28.5–26 Ma, Lipman et al. 1986) have metaluminous, intermediate compositions, ranging from olivine basaltic andesite (53 wt% SiO_2) to quartz latite (67 wt% SiO_2; Johnson and Lipman 1988). Volumetrically subordinate early rhyolites contain as much as 77.5 wt% SiO_2. Chemical zonations in phenocrysts and non-linear variations of many trace-element contents with SiO_2 contents suggest that crystal fractionation was the dominant mechanism for generating the diversity of precaldera Latir rocks (Johnson and Lipman 1988; Fig. 3A and B). Major- and trace-element models and inherited, high-Sr plagioclase in the early rhyolites, for example, suggest that these rocks were derived by crystal fractionation of intermediate-composition magmas similar to those which formed the extensive Latir Peak Quartz Latite. High Mg and Cr contents of augite rims and high whole-rock Ni and Cr contents of some intermediate-composition lavas indicate that these magmas mixed with primitive basaltic magma prior to eruption; the basaltic component mixed in the majority of lavas is ≤ 10 wt% (Johnson and Lipman 1988).

Although no true basalts were erupted within the Latir volcanic field, silicic alkalic and minor tholeiitic basalts were erupted at San Luis Hills, 20 km to the NW, approximately coincident with caldera-forming volcanism at 26 Ma at the Latir field (Thompson and Machette 1989). Chemical compositions of evolved basalts from the San Luis Hills overlap those of the Latir basaltic andesites (Fig. 3) and we consider the overlap of compositions that are too mafic to be derived by crustal melting as evidence for basalt as the magma composition that was parental to the precaldera Latir basaltic andesite, andesite, and quartz latite.

As noted by Johnson and Lipman (1988), the occurrence of quartz and feldspar xenocrysts in some lavas and elevated Pb contents of all Latir rocks (Fig. 3C) indicate that most rocks contain large crustal components. It is unlikely that the intermediate-composition rocks are products of crustal melting alone, because approximately 60% melting of mafic crust would be required (Helz 1976), which appears unlikely.

Inception of alkaline magmatism (alkalic dacite, comendite, and the high-SiO_2 peralkaline Amalia Tuff) coincided with initiation of regional extension at approximately 26 Ma (Lipman 1983; Hagstrum and Lipman 1986; Lipman et al. 1986). The Questa caldera formed 26 Ma ago upon eruption of 500–1,000 km^3 of the Amalia Tuff. Relatively small volumes of peralkaline rhyolite erupted during the later stages of caldera formation are compositionally identical to late-erupted parts of the Amalia Tuff.

Four resurgent plutons, Virgin Canyon, Cañada Pinabete, Rito del Medio, and Cabresto Lake, were emplaced within 1.5 Ma of caldera formation (Lipman et al. 1986; Hagstrum and Lipman 1986; K. Foland, personal communication 1989). The oldest granite is peralkaline and is compositionally identical to late-erupted Amalia Tuff; it crops out along the northern margins of the Virgin Canyon and Cañada Pinabete plutons (Johnson et al. 1989), as a prominant ring dike along the northern caldera margin, and as rare small dikes along the southern caldera margin. Phenocryst compositions in the peralkaline granite suggest that the Amalia Tuff magma evolved from a metaluminous parental magma, rich in alkalies, Ba, Y, Zr, and REE's (Czamanske and Dillet 1988;

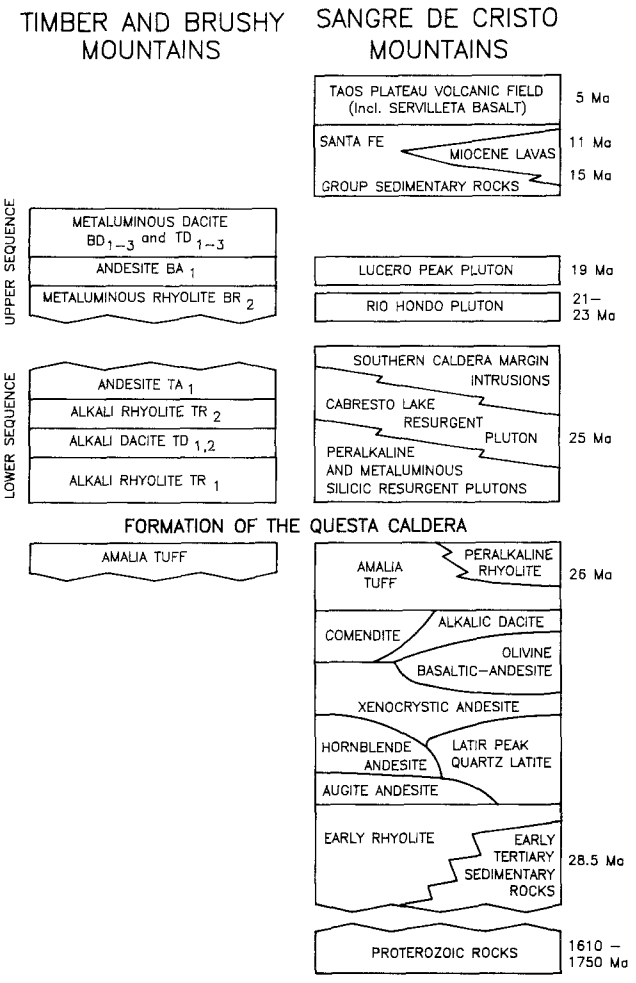

Fig. 2. Stratigraphy of Tertiary igneous rocks exposed in the Sangre de Cristo Mountains (east rift) and Timber and Brushy Mountains (central rift) of northern New Mexico. Revised from Johnson and Lipman (1988) using recently determined $^{40}Ar/^{39}Ar$ ages (K. Foland, personal communication, 1989). Silicic resurgent plutons include Virgin Canyon, Cañada Pinabete, and Rito del Medio. Southern caldera margin intrusions include the Bear Canyon and Sulphur Gulch plutons and the Red River intrusive complex. Stratigraphy of Timber and Brushy Mountains from Thompson et al. (1986)

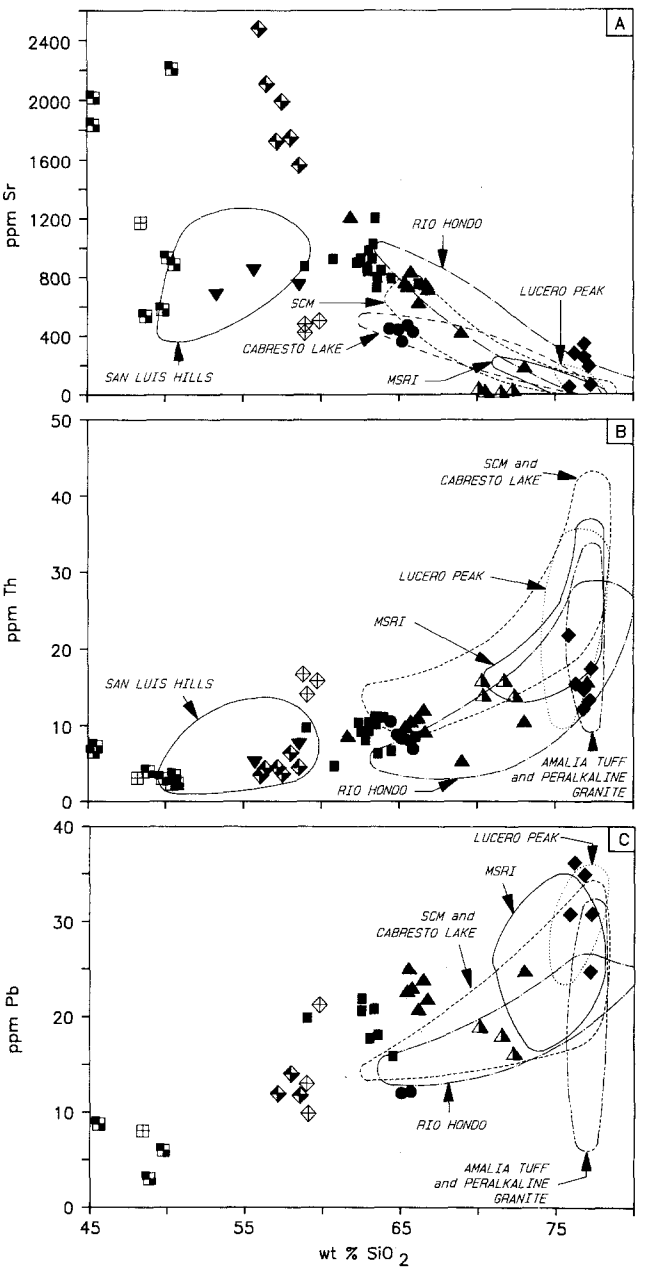

Fig. 3A–C. Selected SiO_2 variation diagrams for volcanic (*symbols plotted*) and plutonic rocks (*outlines only*) of the Latir volcanic field and Miocene lavas (*symbols plotted*) that crop out on the northern flanks of the Latir field. Symbols also plotted for mafic enclaves and a basalt dike associated with the Rio Hondo pluton. Outline of data also shown for San Luis Hills lavas. Data from Johnson and Lipman (1988); Johnson et al. (1989); P. Lipman (unpubl. data), and R. Thompson (unpubl. data). The same symbols are used in subsequent figures. In stratigraphic order: ◈ Miocene andesite; ■ Miocene basalt. Latir intrusions: ▽ Lucero Peak pluton; ⊞ Rio Hondo dikes; ⊕ Rio Hondo mafic enclaves; □ Rio Hondo pluton; ◇ southern caldera margin intrusions; △ Cabresto Lake pluton. Silicic resurgent intrusions: ○ metaluminous granite; ⊕ peralkaline granite. Latir volcanic field: ◍ Amalia Tuff and peralkaline rhyolite; ▲ comendite; ● alkalic dacite; ▼ olivine basaltic-andesite; ▲ Latir Peak Quartz Latite; ■ andesite; ◆ Early rhyolite

Johnson et al. 1989). High halogen fluxes from degassing alkali basalts or crystallizing lower parts of the magmatic system and extensive alkali feldspar fractionation are interpreted as driving forces for establishing the silicic peralkaline compositions.

Early and later facies of silicic metaluminous granite in the Virgin Canyon and Cañada Pinabete plutons, containing high Y, Zr, Ba, and REE contents, were intruded shortly after emplacement of the peralkaline granite; the most mafic sample (2C-41, 71 wt% SiO_2) is considered an appropriate analogue to the parental magma for the Amalia Tuff (Johnson et al. 1989).

Part of the Virgin Canyon pluton and all older volcanic units are tilted northeast (Hagstrum and Lipman 1986). Because the Rito del Medio pluton is not tilted, and continues the differentiation trend defined by metaluminous samples from the Virgin Canyon and Cañada Pinabete plutons (Johnson et al. 1989), the Rito del Medio pluton is interpreted to have crystallized later. The relatively mafic Cabresto Lake pluton, composed largely of monzogranite, was also emplaced during resurgence.

Intrusions emplaced at 25–24 Ma (K. Foland, personal communication 1989) along the southern margin of the Questa caldera are largely alkali-feldspar granite and granite porphyry (Johnson et al. 1989). The two western plutons at Bear Canyon and Sulphur Gulch are the most porphyritic and silicic, and are associated with molybdenite mineralization (Leonardson et al. 1983). The easternmost intrusive units form the Red River intrusive complex.

The youngest plutons of the Latir field, which crop out south of the Questa caldera, include the 22–21 Ma Rio Hondo pluton

Table 1. H and O isotopic data for the Latir volcanic field and associated intrusive rocks

	δD_{WR}[a]	$\delta^{18}O_{WR}$	$\delta^{18}O_{QTZ}$	$\delta^{18}O_{FELD}$	$\Delta^{18}O_{QTZ\text{-}FELD}$	$\delta^{18}O_{MAGMA}$	
Volcanic rocks of the Latir volcanic field							
Latir Peak Quartz Latite							
J-22				6.8		6.8	
J-30				6.8		6.8	
Amalia Tuff							
J-1	−116	11.4	8.1			7.1	
J-2	−120	10.9	8.1			7.1	
J-3	−125	10.5	8.1			7.1	
Plutonic rocks of the Latir volcanic field							
Resurgent plutons:							
Peralkaline granite of Virgin Canyon and Cañada Pinabete							
2C-38	− 87	7.1					
2C-34	− 85	6.1					
2C-49	− 94	7.3					
J-45		6.8[b]	8.5	3.2		7.2	
Early metaluminous granite of Virgin Canyon and Cañada Pinabete							
2C-41	−102	5.9					
2C-40	− 90	7.2					
2C-39	− 96	6.7					
2C-33	− 98	5.3					
Later metaluminous granite of Virgin Canyon and Cañada Pinabete							
2C-35	− 95	8.8					
J-43		4.8[b]	8.0	3.4	4.6	6.5	
Cabresto Lake pluton							
2C-51	− 87	7.5					
2C-51A	− 82	8.2					
J-18		7.4[b]	8.4	7.1	1.3	6.9	
Southern caldera margin intrusions:							
Bear Canyon pluton							
J-37	− 95	7.8	8.9	5.8	3.1	7.4	HJ
2C-8	−105	7.1					HJ
2C-10	−103	5.3					HJ
Sulphur Gulch pluton							
J-36	− 95	5.1	8.3	2.7	5.6	6.8	HJ
2C-52	− 94	2.6					HJ
2C-55	−101	4.0					HJ
J-5 (rhyolite dike)	−110	1.8	8.2	−0.6	8.8	6.7	HJ
Red River intrusive complex							
2C-44	−102	5.6					
J-13		6.3[b]	7.9	5.3	2.6	6.4	

[a] Whole-rock determination except where noted for samples J-12 and J-9

[b] Whole-rock value calculated from mineral modes

[c] Recrystallized quartz. *HJ* = Data from Hagstrum and Johnson (1986) for which chemical analyses are available (Johnson et al. 1989). Additional data reported in Hagstrum and Johnson and plotted in Fig. 5A. $\delta^{18}O_{MAGMA}$ calculated based on unaltered feldspar ($\Delta^{18}O_{Feld\text{-}Magma} = 0$) or quartz in altered samples ($\delta^{18}O_{Qtz\text{-}Magma} = 1.0$ for volcanic rocks, and 1.5 for plutonic rocks; Bottinga and Javoy 1975). Replicate analyses indicate reproductibility of ± 1.5 and 0.2 per mil for H and O isotopic analyses, respectively. Five analyses of NBS-30 (biotite) yield an average δD value of -64.5 ± 2 (1-sigma S.D.) per mil, and twenty analyses of NBS-28 (quartz) yield an average $\delta^{18}O$ value of 9.6 ± 0.2 (1-sigma S.D.) per mil. Analyses of Menlo Park standard plagioclase ST-1 produced an average $\delta^{18}O$ value of 8.4 ± 0.2 (1-sigma S.D.)

Table 1. (continued)

	δD_{WR} [a]	$\delta^{18}O_{WR}$	$\delta^{18}O_{QTZ}$	$\delta^{18}O_{FELD}$	$\Delta^{18}O_{QTZ\text{-}FELD}$	$\delta^{18}O_{MAGMA}$	
Southern plutons of Rio Hondo and Lucero Peak:							
Rio Hondo pluton – granite							
2C-30	− 97	7.3					HJ
J-33	−103	5.2	8.4	4.2	4.2	6.9	HJ
J-34	−103	5.4	8.6	4.1	4.5	7.1	HJ
J-99	− 98	7.6	8.4	6.1	2.3	6.9	HJ
Rio Hondo pluton – granodiorite							
J-8	− 91	6.7	8.4	7.0	1.4	6.9	HJ
J-35	−110	2.9	8.4	0.7	7.7	6.9	HJ
2C-28	−117	6.0					HJ
J-101	−117	5.8	8.5	4.7	3.8	7.0	HJ
J-55	−113	4.4					HJ
J-61	−109	4.8	8.4	3.6	4.8	6.9	HJ
2C-26	−118	5.8					HJ
J-12 (whole rock)	−111	0.2	5.4[c]	−1.2	6.6	−	HJ
J-12 (biotite)	−119						HJ
J-12 (alt. biotite)	−111						HJ
J-12 (hornblende)	−114						HJ
Rio Hondo dikes							
J-9 (alt. biotite)	−123			2.5			HJ
Lucero Peak pluton							
J-7	−100	7.7					HJ
J-46	−103	7.4	9.9	6.1	3.8	8.4	HJ
2C-13	− 99	7.1					HJ
2C-15	−107	8.0					HJ

and the 19 Ma Lucero Peak pluton (Lipman et al. 1986; I. Williams and C. Johnson, unpublished data; K. Foland, personal communication 1988). Composed largely of coarse-grained granodiorite, with minor granite, the Rio Hondo pluton is by far the largest intrusive body exposed in the Latir field, and has the widest compositional variation. Notable features of the Rio Hondo pluton are dissection by hundreds of NW-trending dikes of rhyolite, quartz latite, and basalt, and occurrence in lower exposures of fine- and coarse-grained mafic enclaves. The Lucero Peak pluton contains minor molybdenite mineralization on its eastern margin (Ludington 1981). Both plutons are relatively coarse grained and, although emplaced at structural levels as deep as 5 km below the Miocene surface, are now exposed in their roof zones.

Postcaldera volcanic rocks of the Latir field are not preserved in the Sangre de Cristo Mountains, but are exposed on an intra-rift horst at Timber and Brushy Mountains (Figs. 1 and 2; Thompson et al. 1986). The Cabresto Lake pluton and southern caldera margin intrusions are chemically and temporally similar to the lower lavas on the horst, and the young Rio Hondo and Lucero Peak plutons are chemically similar to the upper lavas (Thompson et al. 1986).

Miocene (15 Ma) basalt and andesite lavas are exposed on the northern flanks of the 29–19 Ma Latir field. Although these rocks are not genetically related to the Latir field, they were erupted during regional block-faulting (Hagstrum and Lipman 1986; Lipman et al. 1986) and are discussed here in the context of isotopic variations in the mantle beneath the northern Rio Grande rift. Two suites can be distinguished based on Sr contents (Fig. 3A) and the low-Sr rocks have chemical compositions that are similar to the 26 Ma San Luis Hills lavas.

Analytical techniques

Representative samples for isotopic analysis were selected from those described in Johnson and Lipman (1988) and Johnson et al. (1989); chemical analyses are tabulated in those reports. All H, O, Pb and most Sr and Nd isotopic analyses were performed in U.S.G.S. laboratories in Menlo Park, CA. Several samples were analyzed for Sr isotope ratios, Rb and Sr contents, and Nd isotope ratios at the University of Wisconsin at Madison. Some of the volcanic rocks are hydrated, and high H_2O content correlates with anomalously high Mg, Ca, and Sr contents. Sanidine separates were used for Sr and Pb isotopic analyses of these samples. Samples containing less than 50 ppm Sr were analyzed by isotope dilution mass spectrometry (IDMS) using a ^{84}Sr spike, and are precise to $\pm 0.2\%$. Samarium and Nd concentrations were determined by IDMS using a total REE spike (including ^{150}Nd and ^{149}Sm spikes) and are precise to $\pm 0.2\%$

Hydrogen for mass spectrometric analysis was extracted by fusing samples at 1400° C and converting the liberated H_2O to H_2 by reaction with U metal at 700° C (e.g., Bigeleisen et al. 1952). Oxygen was extracted by reacting samples with ClF3 at 500° C (Borthwick and Harmon 1982) and reacting the liberated O_2 with graphite at 800° C to produce CO_2 for mass spectrometric analysis. D/H and $^{18}O/^{16}$ ratios are expressed in the standard δ notation where δD and $\delta^{18}O$ values are defined as the relative differences in the sample isotopic ratio and the SMOW (Standard Mean Ocean Water) standard expressed in parts per 1000 ($^0/_{00}$ or per mil). Because whole rocks rarely retain their primary $\delta^{18}O$ values, either because of low-temperature hydration effects in glassy volcanic rocks (e.g., Taylor 1968; Johnson and O'Neil 1984) or sub-solidus hydrothermal alteration (e.g., Taylor 1977), mineral separates were also analyzed. In most cases, magmatic $\delta^{18}O$ values were estimated from O isotopic compositions of quartz, which is highly resistant to O isotopic exchange (e.g., Gregory and Criss 1986), or fresh feldspar.

Strontium was separated by standard ion-exchange chromatography, and mass-analyzed on either a double- or single-collector mass spectrometer at the U.S.G.S., or a six-collector mass spectrometer at the U.W. ("D", "S", or "UW", respectively, Table 2).

Total procedural blanks were <1 ng for U.S.G.S. analyses and <0.1 ng for U.W. analyses, which are all negligible. Rb interference was monitored at mass 85 and was negligible. Random replicate analyses indicate a reproducibility of ±0.00005 (2-sigma S.D.) for the measured $^{87}Sr/^{86}Sr$ ratios for the single-collector mass spectrometer; reproducibility for the double-collector mass spectrometer is generally better, and precision of the six-collector mass spectrometer is ±0.00001. Measured ratios for NBS-987 are identical for all three mass spectrometers within external reproducibility of standards determined on the single collector instrument, and no corrections have been applied to the data.

Initial $^{87}Sr/^{86}Sr$ and $^{143}Nd/^{144}Nd$ ratios were calculated using ages summarized in Lipman et al. (1986) and unpublished $^{40}Ar/^{39}Ar$ ages (K. Foland, personal communication 1989). Errors in initial ratios, potentially large in some rocks with high Rb/Sr ratios, were calculated using a squared-sum partial derivative expression of the decay equation, taking into account the measured errors in the concentrations and isotopic ratios and estimated age (generally ±0.5 Ma). Initial $^{87}Sr/^{86}Sr$ ratios are hereafter referred to as "I_{Sr} ratios".

Neodymium was separated using HCl and 2-methyllactic acid and was mass-analyzed as Nd^+. Total procedural blanks were <0.5 ng for U.S.G.S. analyses and <0.1 ng for U.W. analyses. Initial $^{143}Nd/^{144}Nd$ ratios are reported as ε_{Nd} values relative to the chondrite reservoir (CHUR) at the time of crystallization. The present-day $^{143}Nd/^{144}Nd$ ratio of CHUR is assumed to be equal to that of the BCR-1 standard (Wasserburg et al. 1981). The present-day $^{147}Sm/^{144}Nd$ ratio of CHUR is taken as 0.1967 (Jacobsen and Wasserburg 1980). Most samples were spiked and the accuracy of the corrected $^{143}Nd/^{144}Nd$ ratios was checked by comparing the spike-corrected $^{145}Nd/^{144}Nd$ ratio measured on all samples with that of the average ratio determined on non-spiked standards; no significant differences were noticed. Spike correction of the $^{143}Nd/^{144}Nd$ ratio was usually less than 0.5 ε_{Nd} units.

Lead was separated using HBr and HCl on an anion-exchange column and was mass-analyzed on the single collector mass spectrometer using a mixture of phosphoric acid and silica gel at temperatures of 1200–1400° C. Total procedural blanks were <2 ng. Most samples were analyzed twice under different conditions. Most age corrections for the measured Pb isotope ratios are similar to the analytical uncertainties and the measured ratios are taken as initial ratios.

Results

Stable-isotope data are discussed first, both in terms of primary magmatic compositions and the effects of element mobility during hydrothermal alteration in the upper crust. Radiogenic-isotope data are then discussed in terms of the source(s) of volcanic and plutonic rocks, including the extent to which parental magmas are modified in the lower and upper crust and evaluation of the role of crustal melting.

H and O isotope data

Primary O isotope compositions. The majority of primary (magmatic) $\delta^{18}O$ values for both volcanic and plutonic rocks are relatively restricted, ranging from +6.4 to +7.4 (Table 1 and Fig. 4A). Primary $\delta^{18}O$ values correlate neither with SiO_2 content nor occurrence as volcanic or plutonic rocks. A single sample from the Lucero Peak pluton, the youngest unit in the Latir field, has a primary $\delta^{18}O$ value of +8.4. In contrast, whole-rock $\delta^{18}O$ values range from +0.2 to +11.4 per mil, indicating that both low-temperature hydration (increases in $\delta^{18}O$ values) and high-temperature alteration by meteoric waters (decreases in $\delta^{18}O$ values) has occurred. Whole-rock $\delta^{18}O$ values > +9 are restricted to devitrified samples of Amalia Tuff.

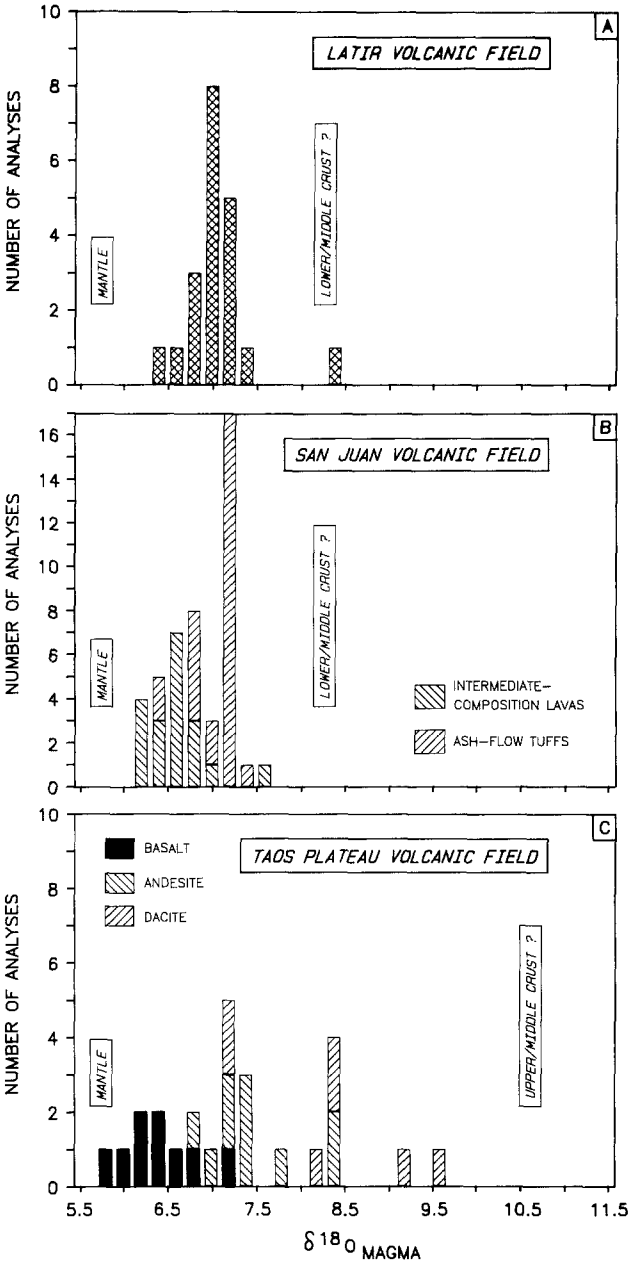

Fig. 4A–C. Histograms of primary $\delta^{18}O$ values for Tertiary volcanic centers in the southern Rocky Mountains. **A** Late-Oligocene to early-Miocene Latir volcanic field (this study, Table 1). Magmatic (primary) compositions calculated based on analyses of unaltered feldspar or quartz. **B** Early-Oligocene to Miocene San Juan volcanic field (Larson and Taylor 1986). Magmatic compositions calculated based on analyses of feldspar, biotite, and quartz. **C** Whole-rock values for the late Miocene to Pliocene Taos Plateau volcanic field (Dungan et al. 1986). Chemical and radiogenic isotope data indicate that magmas at all three volcanic centers assimilated substantial volumes of crust; the differences in $\delta^{18}O$-values are interpreted to reflect interaction with different parts of the crust

Primary $\delta^{18}O$ values for the Latir rocks are similar to those for the San Juan volcanic field (Fig. 4B; Larson and Taylor 1986). Relatively silicic ash-flow tuffs in the San Juan volcanic field tend to have higher primary $\delta^{18}O$ values as compared to those of the more mafic rocks, although

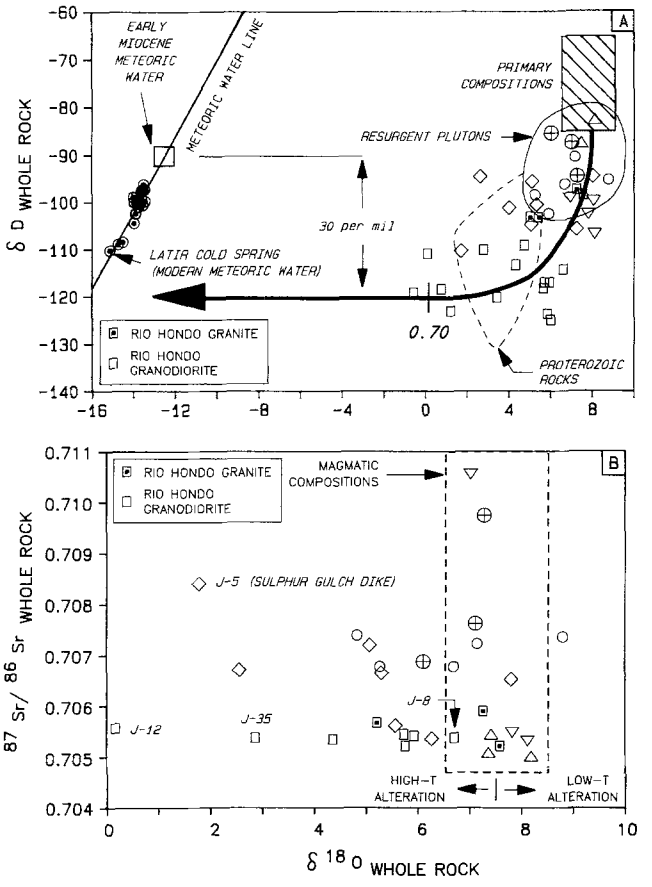

Fig. 5. A δD and δ^{18}O values for Latir plutonic rocks and local modern meteoric waters (⊙). Field for local Proterozoic rocks from Hagstrum and Johnson (1986). Field of primary compositions from Taylor (1977). The whole-rock δD and δ^{18}O values scatter about an isotopic trend (*solid curve*) that is typical of those produced by meteoric-hydrothermal alteration (Taylor 1977); the maximum calculated fluid/rock ratio (atomic) for samples from the Rio Hondo pluton that have low δ^{18}O values is 0.70 (*marked*). See Hagstrum and Johnson (1986) for further discussion. **B** Whole-rock variations in δ^{18}O values and initial $^{87}Sr/^{86}Sr$ ratios (I_{Sr} ratios) for Latir plutonic rocks. Rio Hondo samples plotted in Fig. 6 noted. Field for magmatic compositions calculated from mineral data. J-5 is the only sample that may have undergone a shift in both $^{87}Sr/^{86}Sr$ (increase) and $^{18}O/^{16}O$ (decrease) ratios as a result of high-temperature hydrothermal alteration by meteoric waters that circulated through radiogenic Proterozoic rocks

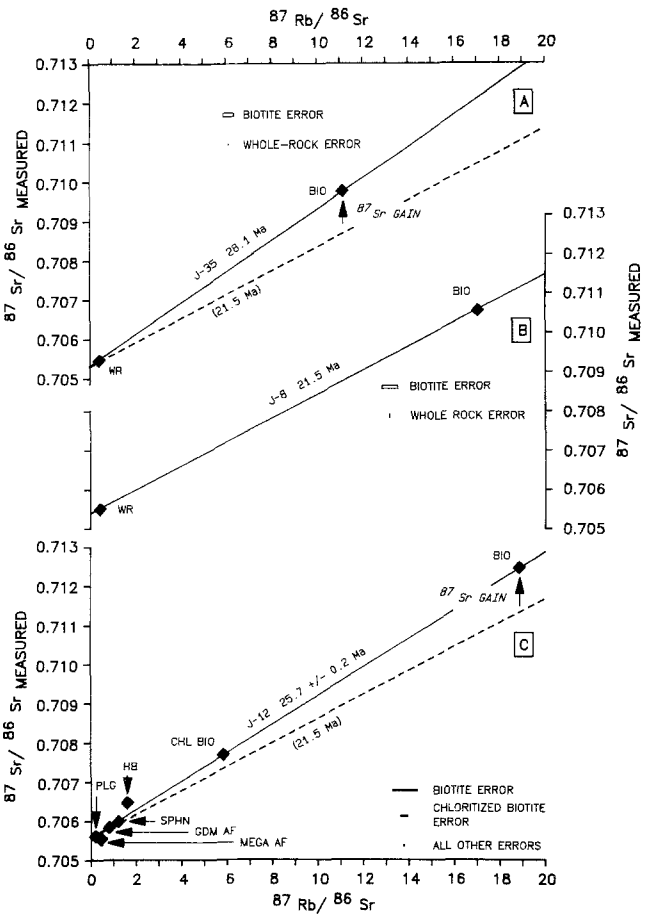

Fig. 6A–C. Sr-isochron diagrams (measured $^{87}Sr/^{86}Sr$–$^{87}Rb/^{86}Sr$) for selected samples from the Rio Hondo pluton. *Large symbols* used for clarity. Analytical error boxes also shown. *BIO* biotite; *WR* whole rock; *CHL BIO* strongly chloritized biotite; *HB* hornblende; *SPHN* sphene; *GDM AF* groundmass alkali feldspar; *MEGA AF* megacrystic alkali feldspar; *PLG* plagioclase. All biotite separates contain some chlorite. **A** Sample J-35. δ^{18}O values for whole rock, quartz, alkali feldspar, and biotite = +2.9, +8.4, +0.7, and −4.4, respectively, indicating extensive exchange with meteoric waters. Anomalously old age is due to incorporation of radiogenic Sr in biotite. **B** Sample J-8. δ^{18}O values for whole rock, quartz, alkali feldspar, and biotite = +6.7, +8.4, +7.0, +2.7, respectively, which approximate primary isotope fractionations (e.g., Bottinga and Javoy 1975). Biotite-whole rock age of 21.5 Ma is similar to the average of incremental heating $^{40}Ar/^{39}Ar$ and zircon U-Pb ages. **C** Sample J-12. δ^{18}O values for whole rock, quartz, and alkali feldspar = +0.2, +5.4, −1.2, respectively, indicating substantial exchange with meteoric waters. Quartz in this sample is recrystallized along internal fractures in the rock; the low δ^{18}O value indicates the presence of magmatic and hydrothermal quartz in the separate

this distinction cannot be made in the Latir field. Given the evidence for significant crustal components in both the San Juan and the Latir magmas (Lipman et al. 1978; this study), the relatively low and restricted primary δ^{18}O values of these centers suggest that the crust involved in both magmatic systems had δ^{18}O values $< +9$, ruling out interaction with supracrustal rocks enriched in ^{18}O (e.g., Taylor 1980).

Whole-rock δ^{18}O values for the largely Pliocene Taos Plateau volcanic field range from +5.8 to +9.6 (Fig. 4C); δ^{18}O values systematically increase from basalt to dacite, suggesting that the Taos magmas can be explained by progressive assimilation of supracrustal rocks relatively rich in ^{18}O (approximately +11 per mil) (Dugan et al. 1986). Although some of the high δ^{18}O values in the Taos rocks may be due to low-temperature alteration of glass, the high δ^{18}O values suggest interaction with unusual supracrustal rocks (high $^{18}O/^{16}O$ but low U/Pb ratios; see below).

H and O isotope compositions of hydrothermally altered intrusive rocks. As previously reported by Hagstrum and Johnson (1986), the Bear Canyon, Sulphur Gulch, and Rio Hondo plutons have been altered by subsolidus interaction with hot meteoric waters. The less drastically lowered whole-rock δD values of the Sulphur Gulch pluton (Fig. 5A), the most strongly mineralized pluton in the Latir field, are probably due to a saline magmatic fluid component, consistent with the alteration assemblages (e.g., Leonardson et al. 1983). The Lucero Peak pluton is relatively unaltered, as indicated by high whole-rock δ^{18}O values and only modest lowering of δD values. The most extensive me-

Table 2. Rb and Sr isotopic data for the Latir volcanic field and associated intrusive rocks

	$^{87}Sr/^{86}Sr$ measured	Rb ppm	Sr ppm	$^{87}Rb/^{86}Sr$	$^{87}Sr/^{86}Sr$ initial	Mass spec
Volcanic rocks of the Latir volcanic field						
Early rhyolites						
J-121AC	0.70665± 4	119	283	1.2164	0.70618± 5	S
J-135B	0.70651± 7	106	194	1.5806	0.70590± 8	S
J-109B	0.71018± 4	140	53	7.6444	0.70725± 10	S
J-117	0.71006± 4	149	68	6.3410	0.70763± 9	S
Augite andesite						
J-113	0.70577± 2	81	855	0.2740	0.70566± 3	S
J-119	0.70566± 5	68	935	0.2103	0.70558± 5	S
Latir hornblende andesite						
J-110	0.70605± 5	58	880	0.1906	0.70598± 5	S
IL-20	0.70563± 7	69	971	0.2055	0.70555± 7	UW
Latir Peak Quartz Latite						
J-22 (plagioclase)	0.70536± 3	16.1	1998	0.0233	0.70535± 3	D
J-PWL	0.70556± 2	148	840	0.5096	0.70536± 2	S
J-125	0.70566± 4	68	645	0.3049	0.70554± 4	S
J-30	0.70596± 7	66	770	0.2479	0.70586± 7	S
J-104	0.70561± 2	75	760	0.2854	0.70550± 2	S
J-116	0.70543± 5	53	745	0.2057	0.70535± 5	S
J-139 (silicic sample)	0.70621± 2	117	202	1.6755	0.70557± 3	S
Xenocrystic andesite						
J-4	0.70512± 3	53	800	0.1952	0.70504± 3	D
J-118	0.70537± 3	88	745	0.3416	0.70524± 3	S
J-123	0.70574± 5	103	930	0.3203	0.70562± 5	S
Alkalic dacite						
J-106	0.70614± 4	82	376	0.6308	0.70590± 4	S
J-114	0.70634± 3	58	482	0.3481	0.70621± 3	S
Comendite						
J-38	0.72686± 2	95	14.02[a]	19.641	0.71960± 18	S
Amalia Tuff						
#1 Camp Creek section, in stratigraphic order						
J-39 (TOP, sanidine)	0.71381± 4	29.39[a]	7.77[a]	10.9503	0.70977± 15	UW
J-41 (sanidine)	0.70799± 2	26.65[a]	19.59[a]	3.9361	0.70653± 5	UW
J-42A (sanidine)	0.70703± 2	85.73[a]	68.57[a]	3.6171	0.70569± 4	UW
4J-204 (sanidine)	0.71087± 2	115.7[a]	25.22[a]	13.2807	0.70597± 11	UW
4J-205 (BASE, sanidine)	0.71447± 4	64.52[a]	12.66[a]	14.7549	0.70902± 16	UW
Miocene lavas						
Hornblende andesite						
J-136	0.70393± 5	44	1750	0.0727	0.70390± 6	S
J-126	0.70420± 2	48.5	1570	0.0893	0.70417± 2	S
J-138	0.70415± 4	42.5	1730	0.0710	0.70412± 4	S
Basalts						
J-107	0.70605± 2	20.5	1820	0.0325	0.70604± 2	S
J-108	0.70479± 3	24	575	0.1207	0.70476± 3	S
J-115	0.70434± 2	19.5	530	0.1064	0.70432± 2	S

$^{87}Sr/^{86}Sr$ ratios normalized to $^{86}Sr/^{88}Sr = 0.1194$. Rb and Sr concentrations by XRF (±2–3% 1-sigma S.D.), except where noted

[a] isotope dilution (±0.2% 1-sigma S.D.) $^{87}Sr/^{86}Sr$ of NBS-987 equal to 0.71023±4 (2-sigma S.E., n=10) for U.S.G.S. double-collector (*D*) mass spectrometer, 0.71029±8 (2-sigma S.E., n=20) for U.S.G.S. single-collector (*S*) mass spectrometer, and 0.71024±1 (2-sigma S.E., n=50) for University of Wisconsin (*UW*) mass spectrometer (multicollector peak-hoping mode). No bias has been applied to the data. Analyses on whole-rocks except where noted. Errors in isotope ratios are reported as ± 2-sigma S.E., where n (number of 10-ratio blocks) equals 4–6 for U.S.G.S. data, and 8–10 for U.W. data

Table 2. (continued)

	$^{87}Sr/^{86}Sr$ measured	Rb ppm	Sr ppm	$^{87}Rb/^{86}Sr$	$^{87}Sr/^{86}Sr$ initial	Mass spec
Plutonic rocks of the Latir volcanic field						
Resurgent plutons:						
Peralkaline granite of Virgin Canyon and Cañada Pinabete						
2C-38	0.71423± 2	122	19.57[a]	18.048	0.70757± 15	S
2C-49	0.80837±35	144	1.58[a]	267.13	0.70972±460	S
2C-34	0.71492± 2	119	15.82[a]	21.778	0.70687± 18	S
Early metaluminous granite of Virgin Canyon and Cañada Pinabete						
2C-39	0.70757± 2	110	150	2.1216	0.70678± 3	S
2C-40	0.70808± 2	117	141	2.4008	0.70719± 3	D
2C-33	0.70743± 2	107	167	1.8537	0.70675± 3	D
Later metaluminous granite of Virgin Canyon and Cañada Pinabete						
2C-35	0.70882± 2	118	86	3.9702	0.70735± 5	S
J-43 (alkali feld)	0.70899± 2	171	116	4.2655	0.70741± 5	D
Rito del Medio pluton						
J-24	0.74992± 2	187	4.62[a]	117.59	0.70700±123	S
Cabresto Lake pluton						
2C-51A	0.70904± 2	210	55	11.048	0.70500± 10	D
J-17	0.70569± 2	112	357	0.9075	0.70535± 2	S
3C-20	0.70629± 2	131	226	1.6768	0.70568± 3	S
J-18 (plagioclase)	0.70520± 2	20.9	304	0.1988	0.70512± 2	D
3C-14	0.70548± 4	103	373	0.7987	0.70519± 5	S
3C-12E enclave	0.70520± 4	92	520	0.5117	0.70501± 4	S
Southern caldera margin intrusions:						
Bear Canyon pluton						
2C-10	0.70766± 2	144	143	2.9134	0.70672± 4	D
J-37	0.71283± 2	248	36.29[a]	19.781	0.70650± 15	S
Sulphur Gulch pluton						
2C-52	0.70834± 2	191	108	5.1170	0.70670± 5	D
J-36	0.71098± 2	214	52.05[a]	11.899	0.70718± 9	S
J-5 Rhyolite dike	0.71172± 2	232	66	10.174	0.70847± 9	D
Red River intrusive complex						
J-16	0.71622± 4	174	17.34[a]	29.056	0.70693± 25	S
J-14	0.70577±11	130	183	2.0549	0.70511± 12	S
J-13	0.70588± 2	116	211	1.5903	0.70537± 3	D
2C-44	0.70563± 2	73	795	0.2656	0.70554± 2	D
Southern plutons of Rio Hondo and Lucero Peak:						
Rio Hondo pluton – granite						
2C-30	0.70841± 3	180	75	6.9442	0.70588± 7	D
J-99	0.70665± 5	146	105	4.0225	0.70518± 8	S
J-33	0.70687± 3	154	132	3.3751	0.70564± 5	S
2C-2	0.70599± 2	100	413	0.7004	0.70573± 2	S
Rio Hondo pluton – granodiorite						
J-8	0.70553± 5	72	520	0.4005	0.70538± 5	S
J-8 (biotite)	0.71060± 4	404.0[a]	68.62[a]	17.038		S
2C-28	0.70548± 2	49.5	580	0.2468	0.70538± 2	D
J-35	0.70548± 2	77	615	0.3621	0.70534± 2	S
J-35 (alt biotite)	0.70977± 5	334.4[a]	86.89[a]	11.137		S
J-55	0.70544± 3	67	735	0.2636	0.70534± 3	S
J-101	0.70546± 4	66	745	0.2562	0.70537± 4	S
2C-26	0.70534± 2	52	1000	0.1504	0.70528± 2	D
J-12 (biotite)	0.71244± 2	288	44.2	18.860		D
J-12 (alt biotite)	0.70771± 2	203	99.8	5.8850		D

Table 2. (continued)

	$^{87}Sr/^{86}Sr$ measured	Rb ppm	Sr ppm	$^{87}Rb/^{86}Sr$	$^{87}Sr/^{86}Sr$ initial	Mass spec
J-12 (hornblende)	0.70645± 2	78.6	136	1.6719		D
J-12 (mega alk fsp)	0.70554± 2	123	791	0.4498		D
J-12 (grnd alk fsp)	0.70582± 2	170	621	0.7918		D
J-12 (grnd plag)	0.70562± 2	34.7	660	0.1520		D
J-12 (sphene)	0.70597± 2	21.4	54.1	1.1442		D
Rio Hondo mafic enclaves						
4J-6E	0.70586± 5	115	428	0.7772	0.70558± 5	S
J-35BE	0.70558± 4	152	500	0.8793	0.70526± 5	S
4J-199E	0.70546± 2	129	491	0.7599	0.70518± 2	S
Rio Hondo dikes						
J-102 (basalt)	0.70560± 5	56	1170	0.1384	0.70555± 5	S
J-131 (qtz latite)	0.70639± 3	80	595	0.3889	0.70625± 3	S
J-9 (rhyolite)	0.70563± 2	129	295	1.2649	0.70516± 3	D
2C-27 (rhyolite)	0.70610± 2	132	108	3.5356	0.70481± 4	D
Lucero Peak pluton						
2C-13	0.72371± 5	215	15.21[a]	40.961	0.71062± 32	D
2C-15	0.70695±33	189	101	5.4137	0.70522± 36	D
J-7	0.70600± 2	121	175	2.0001	0.70536± 3	D

teoric water flow was localized along fractures in the Rio Hondo pluton (Hagstrum and Johnson 1986). Although calculated fluid/rock ratios are highest for the Rio Hondon pluton, this pluton generally appears fresher in hand sample and thin section than the mineralized southern caldera margin intrusions, suggesting that the meteoric fluid which altered the Rio Hondo pluton was relatively dilute. Low δD and $\delta^{18}O$ values of Proterozoic rocks that host the Rio Hondo and Lucero Peak plutons indicate that hydrothermal circulation extended several kilometers outside of the plutons (Hagstrum and Johnson 1986).

Near-magmatic, whole-rock $\delta^{18}O$ values indicate that the resurgent plutons underwent the least meteoric hydrothermal alteration (Table 1), although modest alteration is indicated by slightly lowered whole-rock δD values and moderately large quartz-feldspar fractionations. Precaldera andesitic lavas within the caldera were variably hydrothermally altered, as indicated both by petrologic and isotopic data. These rocks are locally prophylitically altered and hornfelsed to albite-chlorite assemblages; whole-rock $\delta^{18}O$ values range from +0.7 to +6.2 (C. Johnson, unpubl. data). The lowest $\delta^{18}O$ values occur in the central part of the resurgent dome near contacts with the resurgent intrusions. These values are markedly lower than those for the nearby plutons, indicating that extensive meteoric-hydrothermal alteration of the caldera block occurred prior to solidification of the plutons. One andesite from the east caldera margin has a $\delta^{18}O$ value of +7.1, suggesting that no significant meteoric-hydrothermal alteration occurred in this part of the caldera.

The calculated average early Miocene meteoric water composition is $\delta D = -90$ and $\delta^{18}O = -12.5$ per mil (Fig. 5A), assuming a 30‰ fractionation in the D/H ratio between water and rock, appropriate for an integrated exchange temperature of 400–500° C (Suzuoki and Epstein 1976). This calculated Miocene δD value is at least 20‰ heavier than that of average local meteoric water, as measured for a cold spring (Fig. 5A; C. Johnson, unpubl. data). If the integrated exchange temperature was 100° C less than that noted above, the discrepancy becomes 30–40‰. This contrast is similar to that determined using analyses of hydrated volcanic rocks in southern Colorado (see references in Sheppard 1986) and suggests an increase in surface elevation since the early Miocene that is consistent with estimates of 1–3 km of late-Tertiary uplift in the region, based on paleobiological (Axelrod and Bailey 1976) and fission-track data (Kelly and Duncan 1986).

Effects of hydrothermal alteration on radiogenic isotope ratios. We avoided collecting samples that appeared altered in hand sample, particularly from the mineralized Bear Canyon and Sulphur Gulch plutons. Except for one dike sample taken near the Sulphur Gulch pluton (J-5), which has a relatively high I_{Sr} ratio and low $\delta^{18}O$ value, there is no correlation between the extent of high-temperature alteration (as measured by a decrease in *whole-rock* $\delta^{18}O$ value) and the whole-rock I_{Sr} ratio (Fig. 5B). The constancy of *whole-rock* I_{Sr} ratios is particularly striking for samples from the Rio Hondo pluton, where $^{18}O/^{16}O$ ratios of some rocks have been lowered 7‰. Similar relations have been noted in the Idaho batholith (Criss and Fleck 1987). In agreement with earlier work by Dickin et al. (1980), Sr isotope mobility in *whole-rock* samples is generally not a problem, unless low-Sr rocks are extensively altered in the presence of high-saline fluids. The ^{18}O-depleted dike (J-5) has a low Sr content (66 ppm), suggesting that the high I_{Sr} ratio (0.70847) may in part be due to incorporation of radiogenic Sr from the host Proterozoic rocks during hydrothermal alteration.

Three samples from the Rio Hondo pluton that have been variably altered by hydrothermal fluids, based *only* on their whole-rock $\delta^{18}O$ values (all appear relatively fresh in hand sample and thin section), demonstrate that Sr mobility has occurred on the scale of individual minerals (Fig. 6). Recent $^{40}Ar/^{39}Ar$ (K. Foland, personal communication 1989) and U-Pb zircon (I. Williams and C. Johnson, un-

publ. data) age determinations indicate that the Rio Hondo pluton crystallized between 22 and 21 Ma, in agreement with a two-point isochron for sample J8 that has mineral and whole-rock $\delta^{18}O$ values that approximate primary (magmatic) values. In contrast, two samples that have anomalously low whole-rock, feldspar, and biotite $\delta^{18}O$ values have Rb-Sr mineral ages that are too old (samples J-35 and J-12, Fig. 6), suggesting that Sr-poor minerals such as biotite and chlorite (Table 2) have gained radiogenic Sr from the surrounding Proterozoic rocks. Loss of Rb during hydrothermal alteration cannot explain the anomalously old ages, as alteration occurred during cooling of the pluton and there is no evidence for recent alteration that would be required to remove Rb without concomitant changes in $^{87}Sr/^{86}Sr$ ratios due to ^{87}Rb decay. Relatively high Sr contents in the whole-rocks and feldspars have allowed them to retain their primary Sr isotopic compositions.

No correlations are observed between Nd and Pb concentrations or isotopic compositions of whole-rock and degree of alteration, either in hand sample or as indicated by whole-rock $\delta^{18}O$ values (compare Tables 1, 2, 3, and 4). This is consistent with previous studies that indicate Nd to be relatively immobile (Dickin and Jones 1983; Farmer and DePaolo 1987), but contrasts with hydrothermal systems that involve extensive albitization and Pb transport (Dickin and Jones 1983).

Sr isotope data

Precaldera intermediate-composition volcanic rocks have relatively uniform I_{Sr} ratios, in contrast to their varied phenocryst mineralogies; the average ratio, 0.7055 (Table 2), is similar to that measured for evolved lavas at the nearby San Luis Hills. This ratio is identical to the average for slightly older intermediate-composition lavas of the San Juan volcanic field (Lipman et al. 1978), but is significantly higher than that for the younger lavas of the Taos Plateau and Tusas Mountains (avg, 0.7047). Mildly alkalic basalts and hornblende andesites of mid-Miocene age that crop out in the northern part of the Latir field also have low I_{Sr} ratios (avg, 0.7045, suggesting that these represent mantle ratios. One Sr-rich Miocene basanite lava (J-107) has a high I_{Sr} ratio of 0.7061.

Caldera-related rocks vary greatly in I_{Sr} ratio; the comendite has a high I_{Sr} ratio of 0.71960 and I_{Sr} ratios in the Amalia Tuff increase monotonically with decreasing Sr content from 0.70569 to 0.70977 (Fig. 8). These relations generally follow stratigraphic sequence, although correlations are complicated by variations in eruption sequence as inferred by variations in welding sequences. The Sr-poor parts of the Amalia Tuff are thought to represent the earliest erupted parts of the tuff, as inferred by variation in Eu contents (Johnson and Lipman 1988) and comparison with concentration-stratigraphic zonations in other silicic tuffs (e.g., Hildreth 1981). The occurrence of Sr-poor, crystal-rich tuff at the top of the #1 Camp Creek section (Table 2) may reflect eruption of remnant upper parts of the Amalia Tuff magma chamber that underwent extensive glass elutriation. The silicic resurgent intrusions, including the peralkaline granite that continues chemical and mineralogic zonations in the Amalia Tuff, have higher I_{Sr} ratios than the Sr-rich (late-erupted) tuff, suggesting that assimilation of roof rocks occurred after caldera formation.

Fine-grained, porphyritic granite in the Bear Canyon and Sulphur Gulch plutons and Red River intrusive complex has relatively low Sr contents and high I_{Sr} ratios, similar to those for the metaluminous early rhyolite lavas and silicic resurgent intrusions (Fig. 7B). The I_{Sr} ratio for the sample of the Sulphur Gulch pluton reported by Laughlin et al. (1969) falls within the range of values reported here. The coarse-grained, resurgent Cabresto Lake pluton and extracaldera Rio Hondo pluton have relatively constant I_{Sr} ratios, averaging 0.7053, despite a range in Sr content from 50–1000 ppm. This I_{Sr} ratio is similar to the average for intermediate-composition precaldera lavas in both the Latir and San Juan volcanic fields. Two samples from the coarse-grained interior of the Lucero Peak pluton have relatively low I_{Sr} ratios that are similar to those of the Cabresto Lake and Rio Hondo plutons, despite Sr contents as low as 90 ppm. Fine-grained aplite at the roof of the Lucero Peak pluton has a relatively high I_{Sr} ratio of 0.7106.

Nd isotope data

ε_{Nd} values for most Latir volcanic and plutonic rocks vary from -4 to -7 (Table 3, Fig. 9), about midway between chondritic values and values typical of exposed Proterozoic rocks in New Mexico and Colorado (DePaolo 1981a; Nelson and DePaolo 1985; Jacobsen and Wasserburg 1980), although a precaldera basaltic andesite has an ε_{Nd} value of -2. ε_{Nd} values for Latir volcanic and plutonic rocks overlap, and decrease ~ 4 ε_{Nd} units with increasing SiO_2 content. Two rhyolite dikes associated with the Rio Hondo pluton have the lowest ε_{Nd} values in the Latir field, averaging -9. The caldera-related rocks (comendite, peralkaline rhyolite, Amalia Tuff, and peralkaline granite) have ε_{Nd} values that are indistinguishable at -6.5. Analyses of samples from several stratigraphic levels in the Amalia Tuff, including an early vitrophyre and late peralkaline rhyolite lava, confirm that it is homogeneous with respect to Nd isotopic composition. One lithic-rich *bulk tuff* sample has a relatively low ε_{Nd} value of -8; this value is inferred to reflect a mixture of Proterozoic clasts (ε_{Nd}, < -12) and primary tuff ($\varepsilon_{Nd} = -6.5$), although the majority of lithics in the tuff are precaldera volcanic rocks.

The Latir data fall within a trend of decreasing ε_{Nd} with increasing SiO_2 content that is defined by other rocks in the region (Fig. 9A), including basalts. Miocene lavas on the north side of the Latir field generally have higher ε_{Nd} values than those for the Latir field, from -2.5 for a basanite to $+0.2$ for a hornblende andesite. The most primitive tholeiitic and alkalic basalts in the region have ε_{Nd} values between $+1$ and -1; these lavas span an age range of 26 to ~ 3 Ma and include those in the San Luis Hills (26 Ma; C. Johnson and R. Thompson, unpublished data), Tusas Mountains (15 Ma; Williams 1984), Taos Plateau (~ 3 Ma; Williams 1984), and Rayton-Clayton centers (~ 3 Ma; Phelps et al. 1983). These values suggest that the mantle source region for all these mafic volcanic rocks had a relatively uniform ε_{Nd} value of approximately zero.

Pb isotope data

$^{206}Pb/^{204}Pb$ ratios in the precaldera Latir rocks generally decrease with increasing SiO_2 content for mafic- to intermediate-composition rocks, a trend similar to that defined by data from the San Luis Hills and Taos Plateau suites (Fig. 10A). The most primitive lavas in the region, regardless of age, have $^{206}Pb/^{204}Pb$ ratios of approximately 18.2, suggesting that this represents the mantle beneath northern

Table 3. Sm and Nd isotopic data for the Latir volcanic field and associated intrusive rocks

	$^{143}Nd/^{144}Nd$ measured	Sm ppm	Nd ppm	$^{147}Sm/^{144}Nd$	$\varepsilon_{143}(T)$	T_{CHUR} Ma	T_{DM} Ma
Volcanic rocks of the Latir volcanic field							
Early rhyolites							
J-121AC	0.512226± 9	5.62	29.98	0.1133	−7.3±0.2	687	1176
J-135B	0.512358±11	4.58	28.37	0.0976	−4.7±0.2	371	847
J-109B	0.512280±14	4.61	29.11	0.0957	−6.2±0.3	481	932
Augite andesite							
J-113	0.512328±10	6.20	35.72	0.1049	−5.3±0.2	452	945
Latir hornblende andesite							
J-110	0.512311±18	7.18	40.21	0.1080	−5.6±0.4	498	996
IL-20	0.512300± 3[1]				−6.0±0.1[1]		
Latir Peak Quartz Latite							
J-22	0.512248±26	5.14	29.61	0.1049	−6.9±0.5	585	1055
J-PWL	0.512296±12	5.02	28.91	0.1050	−5.9±0.2	506	989
J-139	0.512301±18	3.79	22.16	0.1034	−5.8±0.4	488	968
Xenocrystic andesite							
J-118	0.512325±16	7.30	44.24	0.0998	−5.3±0.3	431	906
Olivine basaltic andesite							
9L-14	0.512517± 3[1]				−1.8±0.1[1]		
Alkalic dacite							
J-114	0.512383±16	10.96	53.58	0.1237	−4.3±0.3	460	1052
J-106	0.512396±11	10.21	50.16	0.1231	−4.0±0.2	429	1024
Comendite							
J-141A	0.512253±14	15.02	93.07	0.0976	−6.7±0.3	532	981
Amalia Tuff							
J-39 bulk tuff	0.512200±31	10.13	38.07	0.1609	−8.0±0.6	1739	2349
J-41P (pumice)	0.512278± 7	12.84	63.41	0.1224	−6.3±0.1	668	1210
4J-204P (pumice)	0.512306±25	11.25	31.78	0.2140	−6.1±0.5	–	–
J-27 (vitrophyre)	0.512264±15	14.45	68.25	0.1280	−6.6±0.3	756	1313
Peralkaline rhyolite							
J-124 (lava)	0.512303±16	5.20	17.58	0.1788	−6.0±0.3	2629	3241
Miocene lavas							
Hornblende andesite							
J-136	0.512505±12	7.04	42.65	0.0998	−1.8±0.2	148	674
J-126	0.512611±29	6.97	42.55	0.0990	0.2±0.6	–	534
Basalts							
J-107	0.512480±10	11.37	69.66	0.0987	−2.5±0.2	197	709
J-108	0.512578± 9	5.37	24.01	0.1352	−0.6±0.2	79	851
J-115	0.512565±18	5.06	22.57	0.1355	−0.9±0.4	112	878

$^{143}Nd/^{144}Nd$ ratios normalized to $^{146}Nd/^{144}Nd = 0.7219$. Sm and Nd concentrations by isotope dilution (±0.2% 1-sigma S.D.), except 4J-6 (INAA). Analyses on whole-rocks except where noted. T_{CHUR} and T_{DM} are model Nd ages calculated relative to chondrite and depleted-mantle reservoirs, respectively (Wasserburg et al. 1981; DePaolo 1981a). $^{143}Nd/^{144}Nd$ of BCR-1 = 0.512618±6 (2-sigma S.E., n=11). $^{143}Nd/^{144}Nd$ of Caltech nNd_{beta} = 0.511900±17 (2-sigma S.E., n=6), which is equivalent to an ε_{Nd} value of −14.0. $^{143}Nd/^{144}Nd$ of Nd lab normal (Ames metal) = 0.512139±11 (2-sigma S.E. n=7), which is equivalent to an ε_{Nd} value of −9.3. Twenty four standard runs produced an average $^{145}Nd/^{144}Nd = 0.348385 \pm 3$ (2-sigma S.E.), which is identical within the external precision error for spike-corrected ratios measured on samples. Errors in isotope ratios are reported as ±2-sigma, where n=15–20 (number of 10-ratio blocks).
[1] Determination at U.W. ($^{143}Nd/^{144}Nd$ of BCR-1 = 0.512620±5 (2-Sigma S.E., n=5); ε_{Nd} (T) calculated using average Sm/Nd ratio of precaldera andesite and quartz latite

Table 3. (continued)

	$^{143}Nd/^{144}Nd$ measured	Sm ppm	Nd ppm	$^{147}Sm/^{144}Nd$	$\varepsilon_{143}(T)$	T_{CHUR} Ma	T_{DM} Ma
Plutonic rocks of the Latir volcanic field							
Resurgent plutons:							
Peralkaline granite of Virgin Canyon and Cañada Pinabete							
3C-23	0.512298±17	26.60	149.9	0.1073	−5.9±0.3	517	1009
2C-38	0.512292±19	10.34	41.30	0.1514	−6.2±0.4	1063	1745
J-94	0.512253±30	8.37	36.12	0.1401	−6.9±0.6	952	1554
Early metaluminous granite of Virgin Canyon and Cañada Pinabete							
2C-40	0.512336±23	8.43	45.00	0.1133	−5.2±0.5	486	1013
Later metaluminous granite of Virgin Canyon and Cañada Pinabete							
J-43	0.512313±18	7.90	42.66	0.1120	−5.6±0.4	520	1034
J-82	0.512355±17	5.00	28.21	0.1072	−4.8±0.3	419	928
Rito del Medio pluton							
J-28	0.512293±22	2.77	21.14	0.0792	−5.9±0.4	394	803
Cabresto Lake pluton							
J-17	0.512365±16	4.28	27.79	0.0931	−4.6±0.3	344	808
3C-12E enclave	0.512393±29	6.56	38.87	0.1020	−4.0±0.6	334	836
Southern caldera margin intrusions:							
Bear Canyon pluton							
2C-10	0.512244±12	3.00	17.37	0.1044	−7.0±0.2	593	1059
J-37	0.512269±13	0.572	3.87	0.0894	−6.5±0.3	471	900
Sulphur Gulch pluton							
2C-52	0.512246±11	2.46	15.69	0.0948	−6.9±0.2	532	970
Red River intrusive complex							
2C-44	0.512338±25	6.50	38.14	0.1030	−5-1±0.5	428	917
J-16	0.512337±17	0.900	6.59	0.0826	−5.1±0.3	348	774
Southern plutons of Rio Hondo and Lucero Peak:							
Rio Hondo pluton – granite							
J-99	0.512263±27	1.06	8.11	0.0790	−6.5±0.5	432	835
Rio Hondo pluton – granodiorite							
J-101	0.512267±15	4.18	27.06	0.0934	−6.5±0.3	490	930
4J-6	0.512304±13	3.5	22.4	0.0944	−5.8±0.3	440	893
Rio Hondo mafic enclave							
4J-6E	0.512320±14	4.85	30.31	0.0967	−5.4±0.3	426	890
Rio Hondo dikes							
J-100 (qtz latite)	0.512277±16	5.37	34.11	0.0952	−6.3±0.3	484	932
2C-27 (rhyolite)	0.512116±16	14.45	68.25	0.1280	−9.5±0.3	1083	1574
J-9 (rhyolite)	0.512157±18	2.92	19.12	0.0923	−8.6±0.4	645	1057
Lucero Peak pluton							
J-7	0.512281±17	2.92	21.76	0.0811	−6.2±0.3	420	831

New Mexico. This ratio is similar to that estimated for the mantle source for Miocene Hinsdale lavas in southern Colorado (Doe et al. 1969).

In contrast, silicic volcanic rocks and several plutons that are exclusively silicic in composition are highly variable in $^{206}Pb/^{204}Pb$ ratio (17.6 to 19.4). Peralkaline rocks have the highest $^{206}Pb/^{204}Pb$ ratios in the Latir field. The Amalia Tuff is zoned from $^{206}Pb/^{204}Pb = 18.82$ near the base (early-erupted) to 19.36 at the top (late-erupted). The peralkaline rhyolite and granite have $^{206}Pb/^{204}Pb$ ratios that are similar to those for the late-erupted Amalia Tuff (as high as 19.45). Analyses of peralkaline granite and early and later metaluminous granite in the resurgent Virgin Canyon and Cañada Pinabete plutons indicate that a significant gap in Pb

Table 4. Pb isotopic data for the Latir volcanic field and associated intrusive rocks

	$\frac{^{206}Pb}{^{204}Pb}$	$\frac{^{207}Pb}{^{204}Pb}$	$\frac{^{208}Pb}{^{204}Pb}$	Pb_{WR} ppm
Volcanic rocks of the Latir volcanic field				
Early rhyolites				
J-121AC	17.999	15.531	37.353	36
J-135B	17.582	15.499	37.246	25
J-109B	18.380	15.571	37.625	31
Augite andesite				
J-113	17.839	15.504	37.388	18
Latir hornblende andesite				
J-110	18.114	15.548	37.632	20
Latir Peak Quartz Latite				
J-22	17.534	15.488	37.229	25
J-PWL	17.673	15.508	37.382	23
J-139	17.453	15.493	37.174	25
Xenocrystic andesite				
J-118	17.553	15.492	37.308	18
Olivine basaltic andesite				
9L-14	17.869	15.478	37.320	
Alkalic dacite				
J-114	17.814	15.509	37.460	12
J-106	17.843	15.518	37.497	12
Amalia Tuff				
J-39 (sanidine)	19.360	15.652	37.886	21
J-41 (sanidine)	18.822	15.618	37.910	18
4J-204 (sanidine)	18.943	15.638	37.951	34
4J-205 (sanidine)	18.902	15.610	37.848	23
Peralkaline rhyolite				
J-124	19.378	15.650	37.956	19
Miocene lavas				
Hornblende andesite				
J-136	17.342	15.457	37.061	14
J-126	17.377	15.469	37.110	12
Basalts				
J-107	18.151	15.529	37.737	9
J-108	18.062	15.546	37.752	6
J-115	18.033	15.513	37.649	3
Plutonic rocks of the Latir volcanic field				
Resurgent plutons:				
Peralkaline granite of Virgin Canyon and Cañada Pinabete				
3C-23	19.116	15.625	37.946	26
2C-38	19.272	15.653	37.938	20
J-94	19.252	15.661	37.928	19
3C-30	19.449	15.659	37.942	
Early metaluminous granite of Virgin Canyon and Cañada Pinabete				
J-93	18.570	15.559	37.590	29
2C-40	18.420	15.579	37.654	26
Latir metaluminous granite of Virgin Canyon and Cañada Pinabete				
J-43	18.463	15.568	37.567	35
J-82	18.432	15.584	37.673	22
Rito del Medio pluton				
J-28	18.412	15.575	37.616	22
2C-22	18.284	15.542	37.557	21
2C-18A	18.246	15.532	37.491	26
Cabresto Lake pluton				
J-17	17.930	15.527	37.418	16
3C-12E enclave	17.962	15.541	37.487	14
Southern Caldera margin intrusions:				
Bear Canyon pluton				
2C-10	18.243	15.563	37.540	24
J-37	17.881	15.527	37.382	34
Sulphur Gulch pluton				
2C-52	18.110	15.551	37.475	21
Red River intrusive complex				
2C-44	17.815	15.526	37.411	21
J-16	18.128	15.543	37.498	18
Southern plutons of Rio Hondo and Lucero Peak:				
Rio Hondo pluton – granite				
J-99	17.575	15.493	37.228	26
Rio Hondo pluton – granodiorite				
J-101	17.500	15.493	37.223	17
4J-6	17.569	15.496	37.243	17
Rio Hondo enclave				
4J-6E	17.558	15.490	37.201	13
Rio Hondo dikes				
J-100 qtz latite	17.526	15.486	37.188	18
2C-27 rhyolite	17.349	15.473	37.137	28
J-9 rhyolite	17.365	15.453	37.053	23
Lucero Peak pluton				
J-7	17.688	15.508	37.173	24

Pb concentrations by XRF (±10% 1-sigma S.D.). Pb isotope ratios corrected using +0.12% per mass unit for mass fractionation based on analyses of NBS-981 and 982. Average internal precision (5–6 10-ratio blocks) is ±0.035% (±0.014% 1-sigma S.D. of the pool of errors). Most samples mass-analyzed in duplicate using separate filaments; average external relative % *difference* in the two analyses is 0.045% (±0.035% 1-sigma S.D. of the pool of errors)

isotopic composition occurs between the closely related peralkaline and metaluminous rocks (Fig. 10B).

The coarse-grained Cabresto Lake and Rio Hondo plutons have relatively constant $^{206}Pb/^{204}Pb$ ratios over a wide range of SiO_2 contents. The Rio Hondo pluton has Pb isotopic compositions that are indistinguishable from those of the precaldera Latir Peak Quartz Latite and may represent a "base-level" composition for intermediate-composi-

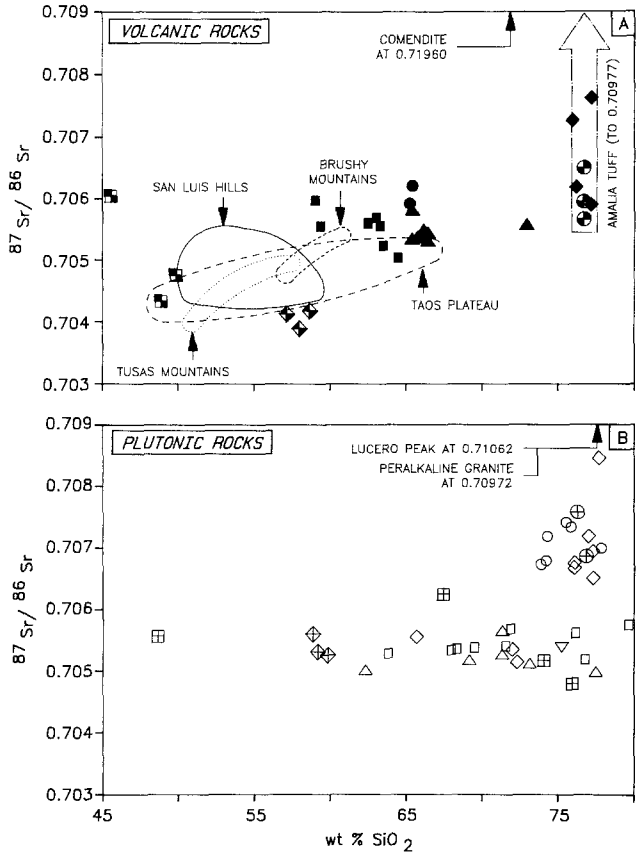

Fig. 7A, B. I_{Sr} ratio – SiO_2 content variations in Latir and Miocene volcanic rocks (**A**) and Latir plutonic rocks (**B**). Data from the San Luis Hills (C. Johnson and R. Thompson, unpubl. data), Brushy Mountain (Williams 1984), Tusas Mountains (Williams 1984), and Taos Plateau volcanic field (Williams 1984; Dungan et al. 1986) suggest similar mantle source and crustal assimilation processes. Intermediate-composition Latir rocks are thought to be products of AFC involving mantle-derived basaltic magmas; temporally-related San Luis Hills lavas may represent magmas that evolved in a manner similar to parental Latir magmas. *Large arrow* in **A** indicates roofward zonation in the pre-eruptive Amalia Tuff magma chamber

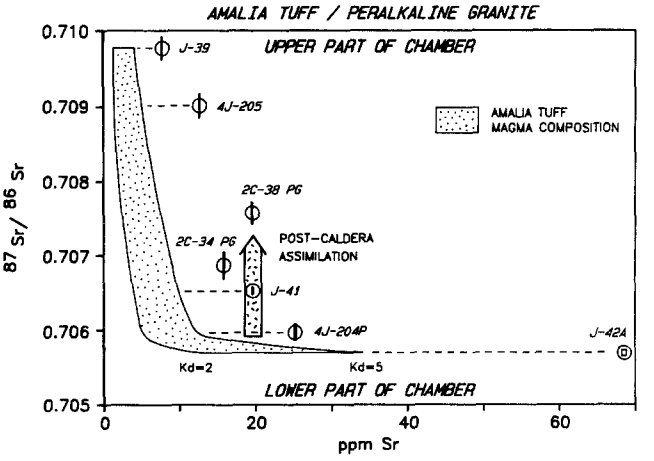

Fig. 8. I_{Sr} ratio – Sr content variations in caldera-related Amalia Tuff and peralkaline granite. Field for magma compositions calculated from sanidine separates from Amalia Tuff (connected with dashed line) using Sr Kd's of 2–5 (see references in Johnson and Lipman 1988). Anomalously high I_{Sr} ratios in peralkaline granite (whole rock values plotted) interpreted as due to assimilation after caldera collapse. *Analytical error boxes* shown; *circles* used for clarity

tion, metaluminous magmas in the Latir field. Two rhyolite dikes associated with the Rio Hondo pluton have the lowest $^{206}Pb/^{204}Pb$ ratios in the Latir field.

$^{207}Pb/^{204}Pb$ and $^{206}Pb/^{204}Pb$ ratios in the Latir field rocks are well-correlated and define a secondary isochron age of 1540 ± 120 Ma that plots significantly above the field for oceanic basalts, but nearly intersects the Stacey-Kramers crustal growth curve (Fig. 11). This age is indistinguishable from the age of the youngest Proterozoic rocks exposed in the Sangre de Cristo Mountains of northern New Mexico at 1620 Ma (Reed 1984). The 26 Ma San Luis Hills basalts have Pb isotopic compositions that overlap those of the Latir field and define the same secondary isochron. Lead isotopic compositions of the Latir rocks overlap the lower range of values measured for Proterozoic rocks from northern New Mexico, which have $^{206}Pb/^{204}Pb$ ratios between 17 and 33 (J. Wooden, C. Johnson, and J. Reed Jr., unpubl. data).

In contrast to relatively systematic $^{206}Pb/^{204}Pb$–$^{207}Pb/^{204}Pb$ variations in the Latir field and San Luis Hills lavas, Pb isotopic compositions of precaldera and caldera-related rocks from the San Juan volcanic field may be divided into several groups of secondary isochrons, varying from 1400 ± 500 to 1970 ± 250 Ma, averaging 1860 ± 110 Ma (Lipman et al. 1978). Compared to the Latir data, most high-precision Si-gel analyses of San Juan rocks have lower $^{207}Pb/^{204}Pb$ ratios at a given $^{206}Pb/^{204}Pb$ ratio, suggesting interaction with crust that had formed in the Proterozoic from reservoirs that had markedly different Pb isotopic compositions from that from which the crust underlying the Latir field and San Luis Hills was generated. Interaction with crust of variable *initial* Pb isotopic composition is indicated for data from the Hinsdale lavas, which define a $^{206}Pb/^{204}Pb$–$^{207}Pb/^{204}Pb$ secondary isochron that is too old to represent a crust formation age.

Peralkaline Latir rocks have anamalously low $^{208}Pb/^{204}Pb$ ratios at relatively high $^{206}Pb/^{204}Pb$ ratios, indicating interaction with crust characterized by exceptionally low Th/U, but high U/Pb ratios. Time-integrated Th/Pb ratios for the source regions of the Latir rocks are less than those of average crust, and U/Pb ratios vary from less than those of average crust to values that are slightly greater, indicating that most Pb was derived from the lower crust.

Discussion

Isotopic variations in the Latir field are broadly similar to those found for other lavas and tuffs in the northern Rio Grande rift region, and suggest that interaction between mantle-derived basalt and crust were also broadly similar. Evolved rocks that are part of largely basaltic lava sequences (i.e., San Luis Hills, Hinsdale Formation, Taos Plateau) have isotopic compositions which are similar to those of intermediate-composition Latir volcanic and plutonic rocks, suggesting that the early and late Latir magmas also evolved through interaction between lower crust and initially basaltic parental magmas. Isotopic compositions of caldera-related magmas in the Latir field indicate interaction with relatively shallow crust, possibly middle crust, a conclusion also reached by Lipman et al. (1978) for the voluminous ash-flow tuffs of the San Juan volcanic field.

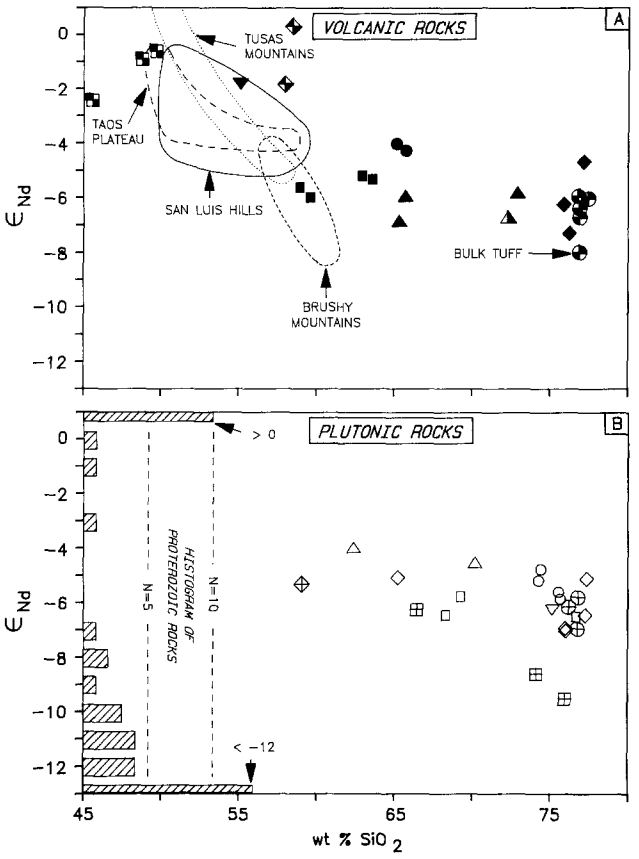

Fig. 9A, B. ε_{Nd} value – SiO_2 content variations in Latir and Miocene volcanic rocks (**A**) and Latir plutonic rocks (**B**). Data from San Luis Hills, Brushy Mountain, Tusas Mountains, and Taos Plateau also shown (sources as in Fig. 7). Anomalously low ε_{Nd} value for one sample of bulk Amalia Tuff interpreted to reflect inclusion of Proterozoic lithic fragments. Histogram of measured ε_{Nd} values of Proterozoic basement rocks in New Mexico and Colorado (**B**, 41 analyses) from DePaolo (1981a) and Nelson and DePaolo (1984; 1985). Few, if any, Latir rocks have ε_{Nd} values that indicate derivation by melting Proterozoic crust, but instead are interpreted as mixtures of mantle-derived basalt ($\varepsilon_{Nd} \sim 0$) and Proterozoic crust ($\varepsilon_{Nd} < -12$)

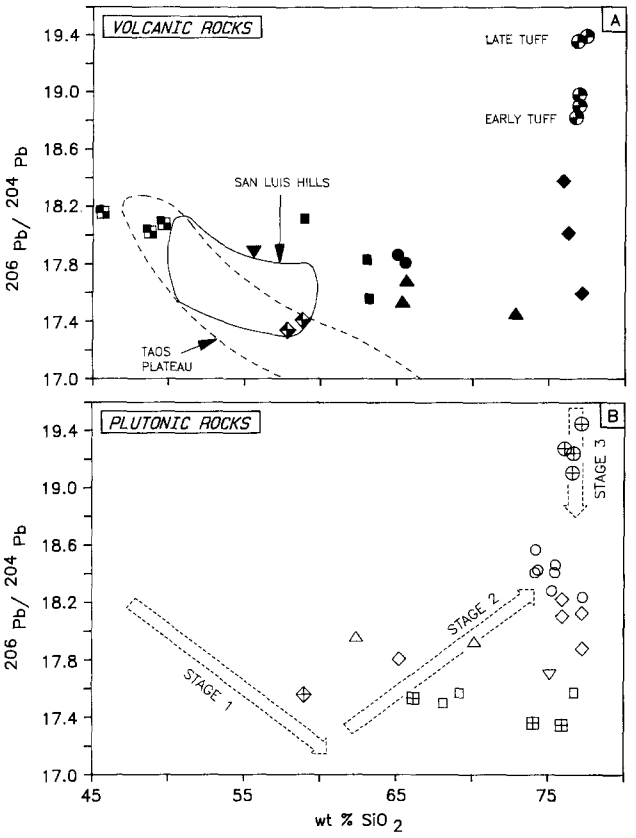

Fig. 10A, B. $^{206}Pb/^{204}Pb$ ratio – SiO_2 content variations in Latir and Miocene volcanic rocks (**A**) and Latir plutonic rocks (**B**). Data from San Luis Hills and Taos Plateau also shown (sources as in Fig. 7). Samples of early- and late-erupted Amalia Tuff taken in stratigraphic sequence indicate that $^{206}Pb/^{204}Pb$ ratios monotonically decreased roofward in the pre-eruptive magma chamber. $^{206}Pb/^{204}Pb$ ratio – SiO_2 variations are interpreted as indicating interaction between mafic parental magmas and relatively nonradiogenic lower crust (STAGE 1) followed by interaction with relatively radiogenic middle crust (STAGE 2). Late assimilation in Amalia Tuff magma chamber interpreted as STAGE 3. See text

Mantle reservoirs

Involvement of primitive basaltic magma in generating the precaldera and post-caldera intermediate-composition rocks is suggested by 1) occurrence of lavas that are too mafic to represent crustal melts, such as the olivine basaltic andesite and late basalt dikes in the Rio Hondo pluton; 2) minimum chemical zonations within plutons from silicic compositions to as little as 64 wt% SiO_2; 3) evidence for mixing between primitive basaltic magmas and evolved magmas (Johnson and Lipman 1988); and 4) chemical and mineralogic relations that indicate crystal fractionation as a major mechanism for producing the intermediate-composition lavas (Johnson and Lipman 1988). The relatively mafic Latir rocks cannot have been produced by "remagmatization" melting of the crust involving variable proportions of restite (e.g., Chappell et al. 1987; Chappell and Stephens 1988) because none of the volcanic rocks and very few of the plutonic rocks contain significant cumulate components (Fig. 3; Johnson and Lipman 1988; Johnson et al. 1989). Isotopic compositions of primitive parental basaltic magma may be estimated from basaltic lavas in the region that have primitive chemical compositions (high-Mg, -Cr, -Ni; low-SiO_2). Based primarily on data from the nearby, temporally-related San Luis Hills center, we estimate that parental basaltic magma contributory to the Latir field had I_{Sr} ratios between 0.7040 and 0.7050, ε_{Nd} values of approximately 0, and $^{206}Pb/^{204}Pb$ ratios of approximately 18.2. The mantle source of this basalt was apparently distinct from that which has underlain the Rio Grande rift for the past few million years in central New Mexico, where alkali and tholeiitic basalts have ε_{Nd} values of +6 to +2 and +5 to −1, respectively (Perry et al. 1987).

Crustal reservoirs and the origin of crustal components in Latir magmas

Relatively low primary $\delta^{18}O$ values and the initial Sr and Pb isotope ratios of intermediate-composition Latir rocks, combined with the petrographic evidence, high Pb contents, and low ε_{Nd} values indicating assimilation, suggest that many of the Latir magmas were contaminated by mafic lower crustal rocks of amphibolite or possibly granulite grade (e.g., Gray and Oversby 1972). Although present-day ε_{Nd} values for Proterozoic rocks in New Mexico and Colorado range from −24 to +14 (DePaolo 1981a; Nelson

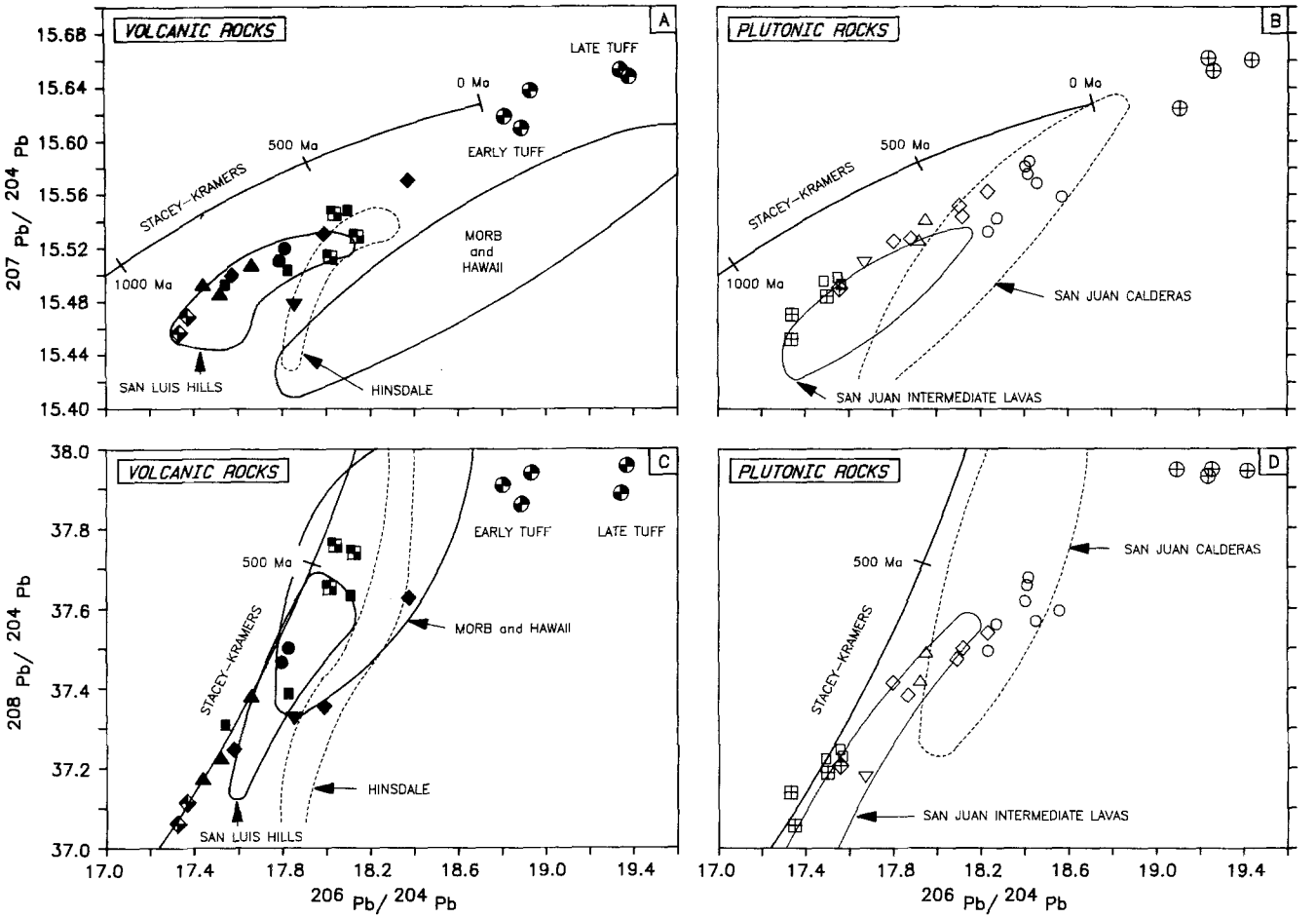

Fig. 11A–D. Pb-Pb isotope variations. Stacey-Kramers average crust evolution curve from Stacey and Kramers (1975). Data from both volcanic and plutonic rocks define a secondary isochron (1540±120 Ma) that passes just right of the Stacey-Kramers curve, but is distinctly above the field for MORB and Hawaiian lavas, and at a lower slope than the field of ash-flow tuffs from San Juan calderas. Data from San Luis Hills (C. Johnson and R. Thompson, unpubl. data), San Juan volcanic field and Hinsdale Formation basalts (Lipman et al. 1978), and MORB and Hawaiian lavas (Dupre and Allegre 1980; Cohen et al. 1980; Cohen and O'Nions 1982; Stille et al. 1983; Staudigel et al. 1984; Hegner et al. 1986) also shown. Some of the variation in $^{207}Pb/^{204}Pb$ ratios for the San Juan rocks due to large analytical errors associated with the PbS-NH_4NO_3 technique (Lipman et al. 1978)

and DePaolo 1984, 1985), the lowest value measured is from a LREE-rich anorogenic granite (GSP-1, DePaolo 1981a) and positive values are found only in some greenstones (Nelson and DePaolo 1984); most values lie between −10 and −14 (Fig. 8B). Measured $^{206}Pb/^{204}Pb$ ratios for Proterozoic rocks range from 17 to 33 (J. Wooden, C. Johnson, and J. Reed Jr., unpubl. data). Less than 5 wt% assimilation of the most radiogenic exposed rocks would markedly increase the $^{206}Pb/^{204}Pb$ ratios of the Latir magmas, suggesting that most crustal interaction occurred in the middle and lower crust.

Increasing I_{Sr} ratios and decreasing ε_{Nd} values with increasing SiO_2 content in basalt-andesite suites in the volcanic sequences of San Luis Hills, Brushy Mountain, the Tusas Mountains, and the Taos Plateau have been interpreted as a result of coupled assimilation/fractional crystallization (AFC; Taylor 1980; DePaolo 1981b) involving mantle-derived basaltic magma (Thompson et al. 1986; Williams 1984; Dungan et al. 1986). The fact that the isotopic and chemical compositions of the basaltic andesite and intermediate-composition Latir rocks overlap those of comparably evolved rocks in the more mafic centers, in addition to evidence for crystal fractionation in the Latir system, strongly suggests that AFC was the primary mechanism for producing the intermediate-composition volcanic and plutonic rocks in the Latir field. Mixing of basaltic and rhyolitic magma cannot have been a major mechanism for producing the intermediate-composition rocks, based both on chemical variations noted above and rheological considerations (e.g., Sparks and Marshall 1986). Moreover, the elevated I_{Sr} ratios of the intermediate-composition rocks cannot be explained by mixing between basaltic magma, with chemical and isotopic compositions similar to those of the San Luis Hills rocks, and silicic magma of the compositions of the Latir early rhyolites, because the markedly lower Sr content of the silicic magma will result in little shift in the Sr isotopic composition of mixtures, unless highly radiogenic I_{Sr} ratios (>0.720) are invoked for the silicic magma.

Neodymium isotope data for the Latir field are best explained by AFC, at a relatively high assimilation:crystallization ratio of 1:2, involving continental crust containing 30–60 ppm Nd with an ε_{Nd} value of approximately −12 and basaltic parental magmas containing 20–30 ppm Nd that initially had an ε_{Nd} value of 0 (similar to primitive lavas from the San Luis Hills; Figs. 12 and 13; Table 5). The Nd and Sr data are well modeled using an I_{Sr} ratio of 0.708 for the Proterozoic crust, although a range of I_{Sr} ra-

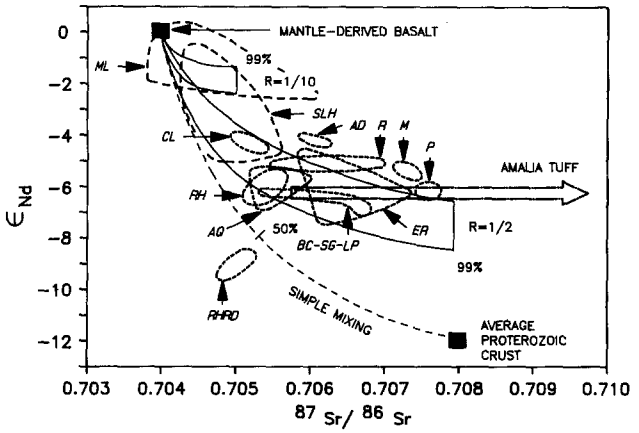

Fig. 12. ε_{Nd} value – I_{Sr} ratio variation for Latir and Miocene rocks. Short-dashed outlines indicate field of data for: *CL* Cabresto Lake pluton; *AD* alkalic dacite; *R* Red River intrusive complex; *RH* Rio Hondo pluton; *AQ* precaldera andesite lavas and Latir Peak Quartz Latite; *BC-SG-LP* Bear Canyon, Sulphur Gulch, and Lucero Peak plutons; *RHRD* Rio Hondo rhyolite dikes; *M* Metaluminous rocks of the silicic resurgent plutons; *P* peralkaline granite. *Dashed arrows* indicate pre-eruptive, roofward zonation of the Amalia Tuff. *Long-dashed outlines* indicate fields of data for: *SLH* San Luis Hills; *ML* Miocene lavas. Simple mixing curve also illustrated (*labeled long-dashed line*) between BASALT ($\varepsilon_{Nd}=0$) and PROTEROZOIC CRUST ($\varepsilon_{Nd}=-12$) endmembers, assuming crust containing 60 ppm Nd and basaltic magma containing 20 ppm Nd. *Solid curves* indicate AFC curves using basaltic magma and crust as endmembers, with assimilation:crystallization ratios (*R*) of 1:10 and 1:2, as marked. Curves end at 99% crystallization. *Upper curves* of the AFC bands are calculated for crust containing 30 ppm Nd. *Lower curves* of the AFC bands are calculated for crust containing 60 ppm Nd. Basaltic magma and crustal Sr contents taken as 1000 and 500 ppm, respectively, for all AFC and mixing calculations. K_d(Sr) and K_d(Nd)=1 and 0.3, respectively. Basaltic magma Nd concentration taken as 20 ppm for AFC curves

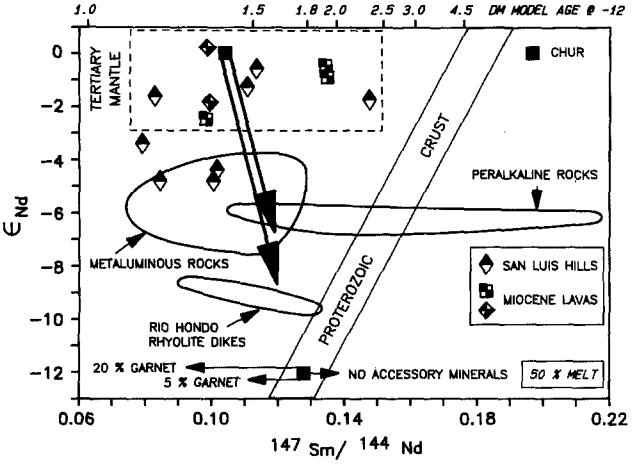

Fig. 13. ε_{Nd} value – $^{147}Sm/^{144}Nd$ ratio relations of data from the Latir field (*outlines*), Miocene lavas (*plotted*), and San Luis Hills (◆ *plotted*). Field of present-day values for Proterozoic crust (circa 1800 Ma) encloses 95% of the data (see also Fig. 9B). Data sources cited in text. *CHUR* denotes average composition of chondritic meteorites (Jacobsen and Wasserburg 1980). AFC trends illustrated (*heavy arrows*) assume basaltic magma endmember has $\varepsilon_{Nd}=0$ and contains 20 ppm Nd, with Sm and Nd K_d's=0.3. Crust composition taken at $\varepsilon_{Nd}=-12$. Both AFC trends calculated using assimilation:crystallization ratio of 1:2 and arrows end at 99% crystallization. *Short arrow* calculated for crust containing 30 ppm Nd, and *long arrow* calculated for crust containing 60 ppm Nd. AFC trends calculated using assimilation:crystallization ratios less than 1:2 generally do not intersect the Latir data (see also Fig. 12). Sm and Nd K_d's for melting calculations from Nicholls and Harris (1980) and Henderson (1982). *Melting arrows* (plotted at $\varepsilon_{Nd}=-12$) calculated for 50% modal equilibrium melting. Source-rock accessory mineral abundances noted. Large ranges in Sm/Nd ratios in the peralkaline rocks solely due to late-stage crystal fractionation. Model Nd ages shown at top, assuming derivation from depleted mantle (DePaolo 1981a) and an ε_{Nd} value of −12

tios and concentrations fit the data; initial crustal interaction probably involved less radiogenic lower crust (Table 5). An important feature of AFC trends is the fact that the low K_d's, appropriate for Nd in mafic magmas (e.g., Henderson 1982), cause ε_{Nd} values in fractionated magmas to quickly attain a "steady-state" value that is higher than that for assimilated crust. This is consistent with the relative constancy of ε_{Nd} values in the intermedidate- to silicic-composition Latir rocks. Production of the intermediate-composition Latir rocks by mixing primitive basaltic magma with crustal melts is *not* consistent with these relations (Fig. 12).

Partial melting of Proterozoic rocks that had an ε_{Nd} (26 Ma) value of −6 (the average of most Latir rocks) is inconsistent with measured ε_{Nd} values for Proterozoic rocks and the REE contents of the Latir rocks. Partial melting of the crust without involving accessory minerals will result in little fractionation of the REEs and would require melts produced from Proterozoic crust with a present-day ε_{Nd} value of −6 to have a $^{147}Sm/^{144}Nd$ ratio of 0.15 (Fig. 13). Although the Amalia Tuff has REE contents that encompass this ratio, REE variations within the tuff are solely due to late-stage differentiation (Johnson and Lipman 1988). Moreover, partial melting involving the common accessory minerals sphene, apatite, and zircon cannot produce the highly fractionated REE compositions observed (Johnson et al. 1989). Large decreases in Sm/Nd ratio during partial melting can only be accomplished by invoking large amounts of residual garnet and unreasonably high degrees of partial melting (>50 wt%, Fig. 13). We further reject an origin by crustal melting for at least the metaluminous Latir rhyolites and granites because petrologic and chemical data suggest that these rocks fractionated from intermediate-composition (and more mafic) parental magmas that are too mafic to be crustal melts (Johnson and Lipman 1988; Johnson et al. 1989). Although there are no clear genetic links between the Amalia Tuff and exposed intermediate-composition rocks, as there are for precaldera rocks and postcaldera plutons, extensive crystal fractionation probably was the primary mechanism for producing the compositional variations within the tuff and also helped to drive evolution of metaluminous parental magma (approx. 71 wt% SiO_2?) to peralkaline compositions (Johnson and Lipman 1988; Johnson et al. 1989). The only rocks that may be direct melts of Proterozoic crust are two anomalous (low ε_{Nd} and $^{206}Pb/^{204}Pb$) rhyolite dikes that cut the Rio Hondo pluton.

Generation of the Amalia Tuff magma by melting precursor Tertiary basalts that had assimilated substantial amounts of Proterozoic crust could explain the Nd-isotope and Pb-concentration data; however, equilibrium partial melting of hornblende-bearing mafic rocks at middle- and lower-crust pressures produces strongly corundum-normative magmas (Helz 1986), inconsistent with the postulated

Table 5. Crystallization and assimilation models for the Latir volcanic field

Major Unit	Exposed/erupted volume (km^3)	Percent crystallization of basalt	Parental basaltic magma	
			Volume[a]/km^3	Ma/Mo[c]
Early rhyolite (*ER*)	50± 10	85±10	333± 232	0.57±0.28
Intermediate-composition lavas (*AND*)	1000± 200	75±10	4000±1789	0.50±0.25
Caldera-related peralkaline rocks (*CALD*)	800± 200	85±10	5333±3797	0.52±0.23
Metaluminous resurgent and southern caldera margin intrusions (*MRES/SCM*)	100± 10	85±10	667± 449	0.57±0.28
Rio Hondo pluton (*RH*)	65± 10	85±10	434± 292	0.57±0.28
Lucero Peak pluton (*LP*)	35± 10	85±10	234± 157	0.57±0.28
Model 1 total:	2050± 283		11000±4252	
Buried plutons[b]	4500±1000	75±10	18000±8237	0.50±0.25
Model 2 total – (*TOT EST PLUTONS*):	6550±1040		29000±9269	

Assimilation/fractional crystallization models and parameters[d]

	ppm Sr	$^{87}Sr/^{86}Sr$	ppm Nd	ε_{Nd}	ppm Pb	$^{206}Pb/^{204}Pb$
Mantle peridotite[e]	10	0.7045	1	0	0.2	18.2
Parental basaltic magma	500	0.7045	20	0	2	18.2
Lower crust (STAGE 1 AFC)	1000	0.7055	30	−12	20	17.0
Average crust (STAGE 2 AFC)	250	0.7080	40	−12	20	20.0
End of STAGE 1 (0–40% crystallization)	800	0.7050	42	− 5	12	17.2
End of STAGE 2 (40–85% crystallization)	100	0.7074	90[f]	− 9	28	19.1

[a] Initial crystallization (40±10%) of parental magmas assumed to form ultramafic olivine and pyroxene cumulates beneath MOHO (STAGE 1, Fig. 14). [b] Lipman 1988. [c] Ma/Mo equal to ratio of mass assimilated (crust) relative to original mass of basalt, calculated using ratio of assimilation:crystallization of 0.375±0.125. [d] See Fig. 14. Calculated assuming assimilation:crystallization ratio of 0.5. STAGE 1 K_d's: 0.8 (Sr), 0.3 (Nd), and 0.5 (Pb). STAGE 2 K_d's: 2.0 (Sr), 0.5 (ND), and 0.7 (Pb). See Johnson and Lipman (1988) and Johnson et al. (1989). [e] Jagoutz et al. (1979). [f] Poor fit not considered important because Nd concentrations in silicic rocks can be substantially lowered due to late-stage crystallization of accessory minerals (Johnson and Lipman 1988; Johnson et al. 1989)
Abbrevations used in Fig. 15 and 16 listed in *italics*

compositions of the parental Amalia Tuff magma (Johnson and Lipman 1988). As noted below, injection of large volumes of mantle-derived basaltic magma significantly lowers Pb *concentrations* in the crust (but does not significantly affect Pb isotope ratios). Markedly lower Pb contents in the late-erupted ("more primitive") parts of the Amalia Tuff (Fig. 3C) are consistent with melting precursor basalts.

Strontium and Pb isotope variations suggest that at least two main stages of crustal interaction were involved in the genesis of the Latir rocks (Figs. 10 and 14, Table 5), with a third stage required for the Amalia Tuff; each stage occurred at a distinct level within the crust. Dungan et al. (1986) note that $^{206}Pb/^{204}Pb$ ratios systematically decrease for the sequence basalt-andesite-dacite in the Taos Plateau volcanic field, accompanied by little change in I_{Sr} ratio, suggesting interaction with relatively non-radiogenic lower crustal rocks. We suggest that the parental basaltic magmas of the Latir field initially evolved by AFC along a trend similar to that of the Taos Plateau magmas, reflecting interaction with lower crustal rocks ($I_{Sr} < 0.705$, $\varepsilon_{Nd} = -12$, $^{206}Pb/^{204}Pb < 17.4$). Latir lavas from this stage did not reach the surface, possibly due to compressional stresses in the crust during precaldera magmatism (e.g., Lipman 1983).

The exposed intermediate- to silicic-composition rocks are best explained as resulting from a second stage of contamination by AFC involving more radiogenic, middle to upper crust (Figs. 10 and 14; Table 5). This second stage involved assimilation of middle- to upper-crustal rocks by intermediate-composition magmas that had been contaminated during stage 1. Finally, we distinguish a third stage of crustal interaction to produce the isotopic *zonation* within the Amalia Tuff magma (Fig. 8), which apparently assimilated Proterozoic rocks characterized by relatively high $^{87}Sr/^{86}Sr$ but low $^{206}Pb/^{204}Pb$ ratios. Limited assimilation in the peralkaline granite occurred after caldera formation (Fig. 8).

Isotopic zonations in Latir magma chambers

Late-stage, roofward contamination of the Amalia Tuff magma, as indicated by Sr and Pb isotope zonations (Fig. 8 and 11), is supported by an increase in the proportion of zircons with Proterozoic cores relative to non-cored Tertiary zircons (in equilibrium with the Zr-rich, mildly peralkaline tuff) toward the base of the Amalia Tuff, as well as by lack of Proterozoic zircon cores in the cogenetic peralkaline granite (Johnson 1989). Calculation of the amount of assimilation effected by the Amalia Tuff magma, using I_{Sr} ratios, is difficult because the low Sr contents of the Amalia Tuff (<20 ppm) make this ratio highly sensitive to contamination. The amount of late-stage crustal assimilation is better constrained by Pb isotope ratios, because Pb contents of the Amalia Tuff are relatively high (10–39 ppm). AFC- or simple-mixing calculations indicate that Proterozoic rocks with high Th/U and low U/Pb ratios, similar to those analyzed by Stacey and Hedlung (1983) from southern New Mexico, appear to be the most likely

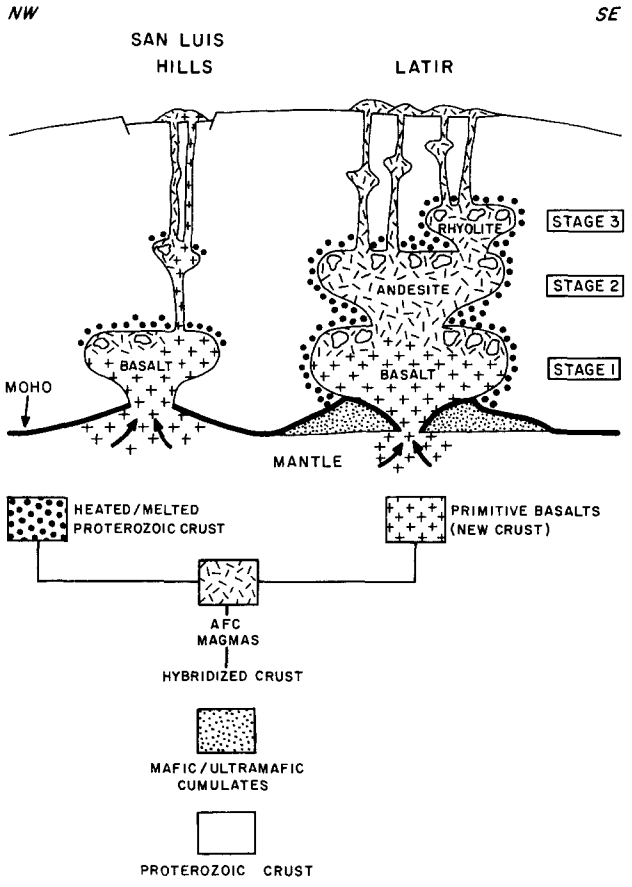

Fig. 14. Cross section through crust and upper mantle depicting extent and locations of Latir and San Luis Hills magmatism. Relatively primitive basaltic and evolved magmas that interact largely with lower crust (STAGE 1) were erupted at San Luis Hills but are rare in the Latir field. Magmatism associated with STAGES 2 and 3 is preserved in the Latir field (see text). Accumulation of mafic and ultramafic cumulates in the lower part of the magmatic system represents return of material to the mantle beneath the MOHO. Cartoon intended to illustrate various stages of Latir magmatism, and not a cross section of the crust after cessation of magmatism

contaminant. These rocks have $^{206}Pb/^{204}Pb$ and $^{208}Pb/^{204}Pb$ ratios (avg, 17.3 and 38.3, respectively) that lie to the left of the Stacey-Kramers curve (Fig. 11C and 11D). Although these compositions are similar to those given by curves for present-day plumbotectonic models of the lower crust (Doe and Zartman 1979; Zartman and Doe 1981), we envision that late-stage contamination occurred in the upper crust, possibly involving supracrustal rocks that may have been depleted in U during diagenesis shortly after deposition.

Although assimilation of crust may occur by melting roof rocks, as recently highlighted by the experiments of Campbell and Turner (1987), the lack of Nd isotope zonation or discontinuity in the Amalia Tuff (or any pluton) precludes this as a significant assimilation mechanism. Given evidence for increasing crystal contents downward in upper-crustal magma chambers and inferred cumulate zones in their lower portions (e.g., Druitt and Bacon 1988), in addition to consideration of high thermal diffusivities in magmas, the heat required for assimilation in the upper portions of such magma chambers is probably driven by crystallization at deeper levels (e.g., Grove et al. 1988; Johnson 1989). Late-stage, roofward assimilation in the Amalia Tuff magma, therefore, is interpreted to have occurred by bulk assimilation, as opposed to AFC or mixing partial melts of the crust.

Approximately 15–20 wt% late-stage assimilation of Proterozoic rocks that had average crustal Pb contents can explain the Pb isotopic variations in the Amalia Tuff, assuming simple mixing as the primary mechanism for incorporation of roof rocks in the phenocryst-poor magma. High Nd contents (30–70 ppm) in the Amalia Tuff preclude large shifts in ε_{Nd} values in the tuff unless there is more than 20–30 wt% assimilation of Proterozoic crust with an ε_{Nd} value of -12, a scenario inconsistent with the relatively uniform ε_{Nd} values in the silicic peralkaline rocks.

Modest increases in I_{Sr} ratio in the porphyritic peralkaline granites of Virgin Canyon and Cañada Pinabete, and in the more evolved porphyritic to fine-grained portions of the Bear Canyon, Sulphur Gulch, and Lucero Peak plutons can be explained by approximately 5 wt% assimilation of Proterozoic roof rocks. This contrasts with homogeneity in Sr and Pb isotope compositions in the coarse-grained Cabresto Lake and Rio Hondo plutons, and in the dominant volume of the Lucero Peak pluton which is also coarse grained. These plutons are zoned to lower Sr and higher Pb *contents* toward their silicic roofs and margins – Cabresto Lake (373–50 and 16–22 ppm, respectively); Rio Hondo (1000–75 and 14–26 ppm); Lucero Peak (175–91 and 24–35 ppm). Although the Sr contents of these plutons are not as low as those in the Amalia Tuff, the Pb contents are generally lower than those in the early tuff, indicating that the Pb isotope compositions of the magmas that solidified as plutons were *more* sensitive to modification by late-stage assimilation of Proterozoic rocks than the Amalia Tuff magma. In light of the highly radiogenic Pb isotope ratios of the Proterozoic rocks intruded by these coarse-grained plutons, it is unlikely that they assimilated Proterozoic crust during the late stages of their magmatic evolution. The relatively uniform ε_{Nd} values that characterize these plutons also suggest that late-stage assimilation did not occur, inasmuch as Nd contents decrease from 28 to 8 ppm toward the granitic margins of the Cabresto Lake and Rio Hondo plutons, making ε_{Nd} values especially susceptible to modification by assimilation.

We suggest that the contrast between evidence for late-stage assimilation in the Amalia Tuff magma and, to a lesser extent, magmas that quenched as porhyritic to fine-grained granite, as compared to the lack of evidence for assimilation in magmas that crystallized to form coarse-grained plutons, is directly related to contrasts in the abundance of crystals in the respective magmas at high levels in the crust, heat content and cooling history of the magma chambers, and, ultimately, flux of basaltic magma into the lower parts of the magmatic system. For example, nearly concordant K-Ar and zircon and apatite fission-track ages (Lipman et al. 1986) in the resurgent plutons and the relative lack of meteoric-hydrothermal alteration in the plutons as compared to the host andesites, suggests that these plutons cooled relatively rapidly and had minimal time to assimilate roof rock. The larger isotopic variations in fine-grained parts of the Bear Canyon, Sulphur Gulch, and Lucero Peak plutons, and greater inferred assimilation of roof rocks may be a result of slightly slower cooling at somewhat greater depths.

In contrast, deeper parts of the magma chambers, now represented by coarse-grained rocks of the Cabresto Lake and Rio Hondo plutons may have had little opportunity to assimilate roof rock because they represented the uppermost portions of crystal-rich systems. Strongly discordant conventional K-Ar and fission-track ages for samples of the Rio Hondo granodiorite (Lipman et al. 1986) suggest that the magma was crystal rich and near its solidus for an extended period (e.g., Spera 1980). In comparison to its granitic facies, the deeper, granodioritic portion of the Rio Hondo pluton has markedly lower quartz-magnetite oxygen-isotope temperatures and has undergone more extensive hydrothermal alteration (Hagstrum and Johnson 1986), suggesting that it cooled significantly more slowly than the upper granitic portion. These factors suggest that the total heat available for assimilation in the upper part of the crystal-rich portion of the Rio Hondo magma chamber was relatively low, consistent with the lack of isotopic zonation in the pluton. If stoping and sinking of roof blocks is the dominant mechanism for assimilation, there is probably a limit to the crystal content through which the blocks can sink, effectively precluding assimilation.

Effects of magmatism on chemical and isotopic compositions of the crust and lithospheric mantle

Voluminous basalt injection as a general requirement for the origin of caldera complexes and large-volume volcanic fields. The combination of sustained (as much as 15–20 m.y. duration) eruption of magma with generally low crystal contents at some magmatic centers and the common occurrence of recurrent caldera forming eruptions of highly evolved magma over relatively short time intervals (<1–2 m.y.) has led many workers to suggest that a general requirement for developing caldera complexes is a large flux of mantle-derived basaltic magma into the lower parts of the magmatic system. This basaltic magma provides the heat and mass required to evolve silicic, largely liquid magmas at high levels within the crust and to sustain magmatism for long periods of time (e.g., Christiansen and Lipman 1972; Smith 1979; Hildreth 1981; Spera and Crisp 1981). Geophysical data provide evidence for large partial melt zones extending into the mantle beneath recent calderas (Eaton et al. 1975), presumably reflecting large volumes of basaltic magma.

Crystal fractionation was important during evolution of the Latir magmas, and the chemical and isotopic compositions of the metaluminous intermediate- to silicic-composition volcanic and plutonic rocks are well explained by AFC involving basaltic parental magmas. Generation of the silicic peralkaline units and development of compositional gradients in the Amalia Tuff magma also was in part due to extensive crystal fractionation, although halogen fluxing and other processes (e.g., Macdonald and Smith 1988) probably had a significant affect (Johnson et al. 1989). Substantial volumes of basaltic magma were required to generate the Amalia Tuff magma, regardless of whether it originated by AFC of basaltic parental magmas or partial melting of contaminated precursor basalt/andesite, For example, to generate the chemical and isotopic compositions of the tuff, a 5–25 wt% partial melt of precursor basalt/andesite would require essentially the same volume of basalt as 75–95% AFC of a basaltic parental magma (Table 5).

Recent Nd isotope data for silicic rocks in volcanic centers erupted through Proterozoic crust in the southwestern U.S. support a model for substantial basaltic components in large magmatic systems: the Kane Springs Wash caldera ($\varepsilon_{Nd} = -5$ to -7, Novak 1985), McDermitt and Silent Canyon calderas ($\varepsilon_{Nd} = +3$ and -5, Tegtmeyer and Farmer 1987), Woods Mountain volcanic field ($\varepsilon_{Nd} = +2$ to -7, Musselwhite et al. 1989), Mount Taylor volcanic field ($\varepsilon_{Nd} = -2$, Perry et al. 1983), Jemez volcanic field ($\varepsilon_{Nd} = -1$ to -4, Loeffler and Futa 1985), and possibly the Timber Mountain caldera (Tegtmeyer and Farmer 1987; G. Farmer, personal commun. 1988). Cenozoic silicic volcanic rocks in eastern Mexico have ε_{Nd} values of $+1$ to -2 (Verma 1983, 1984; Cameron and Cameron 1985), significantly higher than those for exposed Proterozoic rocks (Patchett and Ruiz 1987). In contrast, silicic volcanic rocks in western Mexico are probably underlain by Phanerozoic basement, and have relatively high ε_{Nd} values of 0 to $+5$ (Cameron and Cameron 1985; Mahood and Halliday 1988). The majority of rhyolites erupted from the Yellowstone caldera have ε_{Nd} values near -9, which is markedly higher than the average of Archean crust through which the magmas were erupted (Halliday et al. 1986). Exposed plutons associated with cogenetic volcanic rocks in the Latir field are inferred to represent an underlying batholith, based on gravity measurements (Lipman 1988). Lipman (1984) emphasized the association of large volumes of plutonic rocks with volcanic centers. General models of magmatism suggest that volumetric ratios of plutonism to volcanism are approximately 10:1 (Crisp 1984; Shaw 1985), indicating that the extent of basaltic magma injection calculated from volumes of volcanic rocks alone are probably minimums.

Implications for modification of the crust and lithospheric mantle. Significant crustal thickening, hybridization, and compositional changes occur in the crust and upper mantle during evolution of large magmatic centers that are generated and sustained by high fluxes of mantle-derived basaltic magma into the crust. Using petrologic and isotopic constraints on the percentages of crystallization and relative proportions of parental basaltic magma and crust involved in generating the major units in the Latir field (Table 5), we consider estimates of the percentages of crystallization required to 1) produce the exposed volume of volcanic and plutonic rocks (model-1 "LP" stage, Figs. 15 and 16, Table 5) and 2) produce the exposed volume of volcanic and plutonic rocks, as well as the volumes of low-density plutonic rocks inferred to inderlie the Latir field, based on gravity data (model 2- "TOTAL EST PLUTONS" stage, Figs. 15 and 16, Table 5; Cordell et al. 1986; Lipman 1988). Between 11000 ± 4000 km^3 (model 1) and 29000 ± 9000 km^3 (model 2) of mantle-derived basaltic magma was involved in the Latir magmatism (after individually propogating all errors for each model, Table 5). Given that the low density plutonic rocks that are inferred to underlie the Latir field probably have intermediate- to silicic-compositions, we consider model 1 to be an extreme lower limit, and model 2 to be more representative.

These large volumes of mantle-derived basaltic magma probably pooled near the Mohorovićić seismic discontinuity (MOHO), given O, Sr, and Pb isotope data that indicate substantial interaction with the lower crust. Volume and compositional calculations assume that early crystallization ($40 \pm 10\%$; Table 5) of olivine and pyroxene oc-

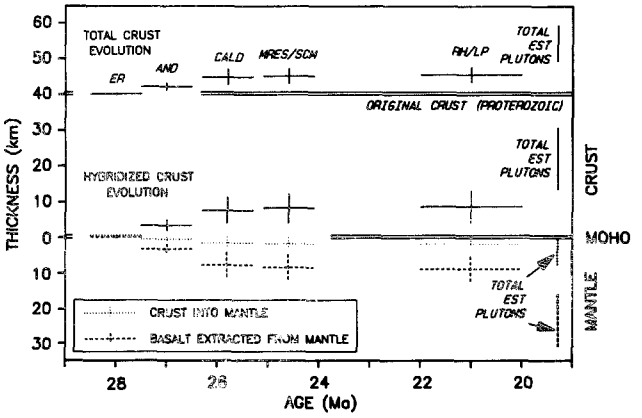

Fig. 15. Time-related variations in thickness and volume for total crust and hybridized crust for the Latir volcanic field. Abbreviations, initial conditions, and estimated errors for calculations listed in Table 5. Initial crustal thickness is assumed to be 40 km (Lipman 1988) and locus of magmatism is assumed to be restricted to 1200 km^2 area. Hybridized crust is defined as the sum of new crust (components of mantle-derived magmas remaining in the crust) and pre-existing Proterozoic crust that has been assimilated. Error bars indicate sum of propogated errors in volume estimates and errors in age determinations for the major units. *ER*, *AND*, *CALD*, *MRES/SCM*, *RH*, and *LP* labels here and in Fig. 16 represent calculated evolution accompanying units (Model 1, Table 5). *TOTAL EST PLUTONS* labels here and in Fig. 16 include exposed units and estimates for buried plutons (Model 2, Table 5). *Vertical bars* on right side of figure indicate final values for Model 2

curred near the MOHO, and that the resulting cumulate zones lay beneath the MOHO (Fig. 14). These cumulate zones substantially reduce difficulties such as large-scale uplift that should be associated with the crustal thickening that would accompany injection of 11000 to 29000 km^3 of basaltic magma into the crust. Moreover, if accompanied by crustal assimilation, early crystallization and cumulate formation provides a mechanism for transferring crustal components into the upper mantle. Finally, we define the hybridized crust as the sum of 1) the mass of Proterozoic crust that was assimilated by magmas that remained in the crust and 2) the mass of relatively fractionated magma that remained in the crust following early olivine and pyroxene crystallization. It is important to note that although the geologic and petrologic evolution of the Latir field is reasonably well-constrained, many parameters involved in the volume and compositional calculations are not (Table 5, Figs. 15 and 16). Our emphasis is on the general trends in chemical and isotopic compositions of the crust and upper mantle.

Assuming that inferred magma volumes underlay an area of 1200 km^2, crustal thickness increased between 5.5±2.2 km (model 1) and 14.5±4.9 km (model 2) during Latir magmatism. The thickness of hybridized crust at the end of Latir magmatism ranged from 8.5±4.6 km (model 1) to 22.0±8.6 km (model 2). AFC that occurred during the initial 30–50% crystallization of parental magmas at the MOHO resulted in a net transfer of 2.0±1.6 km (model 1) to 5.0±3.6 km (model 2) of crust into the upper mantle. Spread under the 1200 km^2 area of the Latir field, the total volume of basaltic magma extracted from the upper mantle (not including cumulates returned) is equivalent to 9.2±3.6 km (model 1) to 24.2±7.7 km (model 2) thickness of material. For purpose of illustration, we have chosen

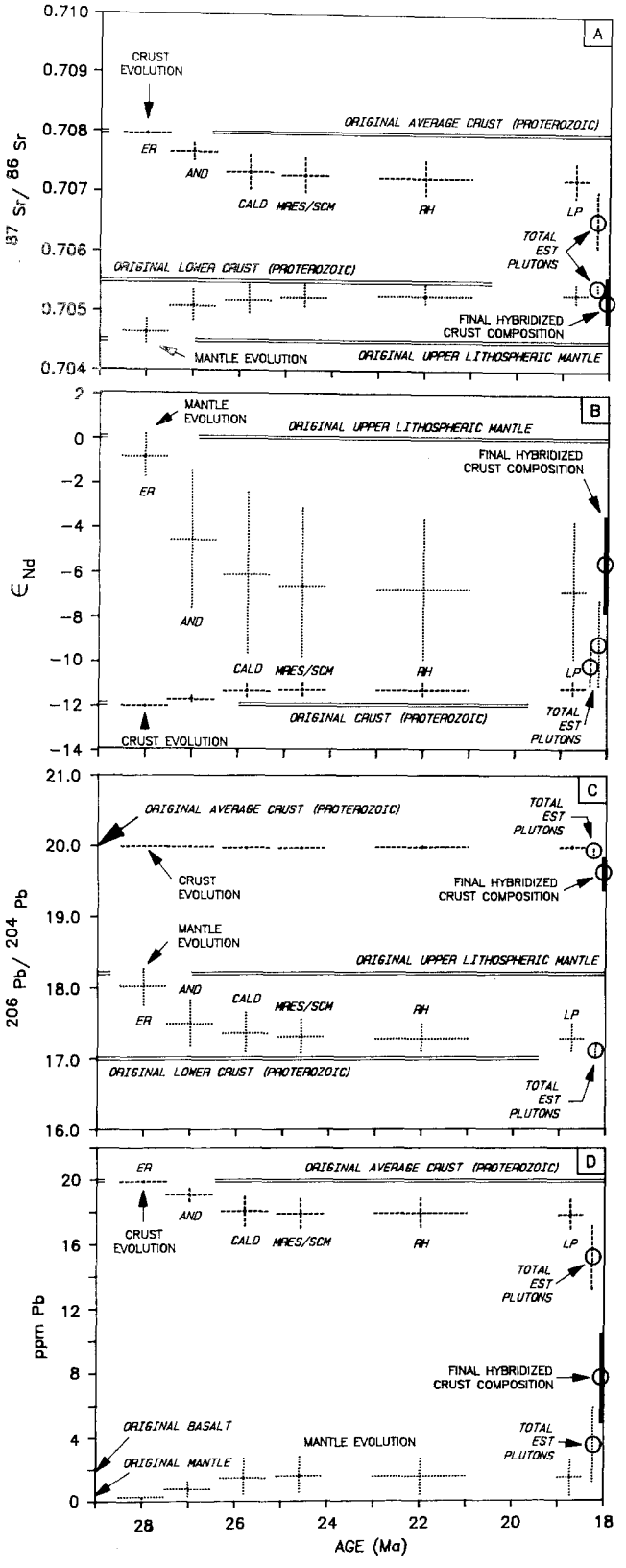

Fig. 16A–D. Compositional variations in total and hybridized crust and upper mantle, with time, for the Latir field. Calculations based on volumes calculated for Fig. 15. Isotopic, concentration, and K_d parameters listed in Table 5. *Error bars* calculated by propogation of errors noted in Table 5. *Vertical bars with circles* on right side of figures indicate final compositions for Model 2. **A** $^{87}Sr/^{86}Sr$ ratios; **B** ε_{Nd} values; **C** $^{206}Pb/^{204}Pb$ ratios; **D** Pb concentrations

24.2 km to represent that portion of the upper mantle involved in crustal recycling during initial crystallization at the MOHO.

Model calculations indicate that $^{87}Sr/^{86}Sr$ ratios for the total crust may drop 20 ± 9 (model 1) to 40 ± 14 (model 2) percent closer to that of the mantle, whereas the average $^{87}Sr/^{86}Sr$ ratio for the hybridized crust may drop 80 ± 11 percent closer (Fig. 16A). $^{87}Sr/^{86}Sr$ ratios for the upper mantle (24.2 km beneath the MOHO in our model) may increase 80 ± 20 (model 1) to 90 ± 10 (model 2) percent closer to that of the lower crust during initial crystallization at the MOHO (Fig. 16A). ε_{Nd} values for the total crust rise only slightly toward that of the mantle, between 7 ± 3 (model 1) and 16 ± 8 (model 2) percent, and the average ε_{Nd} value for the hybridized crust may increase 53 ± 18 percent closer (Fig. 16B). ε_{Nd} values for the upper mantle may drop 57 ± 26 (model 1) to 77 ± 17 (model 2) percent closer to that of the crust (Fig. 16B).

The shift in Pb isotope ratios for both the total and hybridized crust is relatively small, primarily because injection of mantle-derived basaltic magma involves low Pb fluxes into the crust. $^{206}Pb/^{204}Pb$ ratios for the total crust drop only 1 to 4 percent closer to that of the mantle and the hybridized crust drops $22\pm12\%$ closer (Fig. 16C). In contrast, Pb isotope ratios in the upper mantle drop 77 ± 18 (model 1) to 91 ± 3 (model 2) percent closer to that of the lower crust (Fig. 16C). Despite large uncertainities in the volume of initial basaltic magma and assimilation:crystallization ratios, the calculations demonstrate that injection of large amounts of mantle-derived basaltic magma into the crust results in little change in the Pb isotopic composition of the pre-existing crust. Injection of mantle-derived basaltic magma into the crust largely dilutes average Pb concentrations; model calculations indicate that total crustal Pb concentrations may drop 11 ± 5 (model 1) to 24 ± 11 (model 2) percent closer to that in the parental *basaltic magma*, and that Pb concentrations in the hybridized crust may drop 68 ± 16 percent closer (Fig. 16D). If any significant crystal accumulation occurs near the MOHO during AFC, however, the low Pb (and Sr and Nd) contents of the upper mantle allow addition of relatively small volumes of crust to almost completely overprint original mantle isotopic compositions with crustal isotopic compositions.

The calculations illustrated in Figs. 15 and 16 indicate that the lower crust beneath large-volume volcanic centers may largely consist of hybridized crust that contains multiple basaltic intrusions which have undergone mixing, assimilation, and crystallization. In terms of surface uplift, mafic and ultramafic rocks crystallized in the lower crust and upper mantle may largely offset the effects of net additions to the crust. Generation of ultramafic cumulates beneath the southern Rocky Mountain volcanic centers may explain the comparable depths to the MOHO under the Great Plains and southern Rocky Mountains (Prodehl and Lipman 1989). Late-Tertiary uplift, as indicated by other studies and data discussed here, probably is related to recent lithospheric processes (Bird 1984; Lipman 1988), as opposed to the magmatic processes discussed for the Latir field. Anomalously low seismic velocities in the middle crust beneath the Latir field, in comparison to crust beneath the Great Plains to the east (Prodehl and Lipman 1989), may provide evidence for extensive hybridization in the middle and uppper crust in the form of extensive intermediate- to silicic-composition intrusions. Our model is similar to the "MASH zone" proposed by Hildreth and Moorbath (1988), although they call upon crustal melting as a more important process. Compressional tectonics may promote crustal melting, and this is an important contrast between the tectonic setting of the Latir field, for which our model has been developed, and the Andean arc environment for which Hildreth and Moorbath (1988) developed their model.

Chemical and isotopic analyses of evolved rocks at long-lived volcanic centers can provide important tests of our model. For example, as a magmatic system evolves, a greater proportion of evolved magmas should have relatively primitive isotopic compositions. This will be reflected in magmas that either assimilate hybridized crust, or are generated from it by crustal melting. Moreover, our model predicts major changes in the Sr and Nd (*but not Pb*) isotope compositions and Pb *concentrations* of progressively younger magmas derived by crustal melting or assimilation. If the crust is largely composed of supracrustal rocks enriched in ^{18}O, late crustal melts should have substantially lower $\delta^{18}O$ values as a result of continued mantle input into crust that is melted/assimilated. This trend was observed in Tertiary rhyolites of the Sonoma/Tolay volcanic field in western California (Johnson and O'Neil 1984).

Summary and conclusions

Geologic, geophysical, and petrologic constraints provide a detailed model for magmatic evolution of the Latir magmatic system which addresses questions regarding: 1) roles of the crust and mantle in generation and evolution of the magmas, 2) sections of the continental crust involved in magmatism, and 3) conditions under which the chemical and isotopic compositions of magmas may be modified at high levels within the crust. Most Latir rocks represent magmas that underwent two stages of assimilation: 1) assimilation by basaltic parental magmas of lower crust that had relatively non-radiogenic $^{206}Pb/^{204}Pb$ ratios (<17.3), and 2) assimilation of middle- and upper-crustal rocks that had relatively radiogenic $^{206}Pb/^{204}Pb$ ratios (>19.5) by intermediate-composition magmas that had been contaminated in the lower crust. No rocks representing purely stage 1 assimilation are exposed in the Latir field; model calculations and comparison with regional volcanic fields that dominantly contain mafic rocks suggest that stage 1 magmas represent initial 30–50% crystallization of parental basaltic magma. Evidence for this stage is inferred by comparison of isotopic variations in Latir rocks of basaltic-andesite to quartz latite compositions, with data for mafic- to intermediate-composition volcanic centers in the region, particularly the temporally related San Luis Hills. A third stage of assimilation, restricted to high levels in the crust, is indicated for magmas that formed the Amalia Tuff and porphyritic to fine-grained silicic rocks. Coarse-grained plutons crystallized from crystal-rich portions of the magmatic system; hence, relatively little additional heat, required for assimilation at high levels, could be generated by further crystallization. Despite this contrast in high-level evolution, the majority of both volcanic and plutonic rocks of the Latir field originated by fractionation of large volumes of parental basaltic magma that had assimilated substantial volumes of crust. A critical factor in this interpretation is establishment of genetic relations between fractionated and

relatively mafic rocks (basaltic andesite) that are too mafic to be crustal melts. The lack of true basalts exposed within the locus of Latir magmatism may be due to the presence of large volumes of silicic magma. Interpretations based on analyses of the silicic rocks alone are, therefore, ambigous.

Injection of large volumes of basaltic magma may substantially change the isotopic and chemical composition of the total crust, may effect even larger changes in the volume of crust that represents a hybridized mixture of mantle and pre-existing crust, and may significantly modify the isotopic composition of the upper mantle. We note that models for the origin of silicic rocks, whether by melting of precursor basaltic rocks that have been contaminated, or by AFC involving basaltic parental magmas, require injection of mantle-derived basaltic magma that is approximately 10 times the volume of the silicic rocks. To the extent that large volumes of basaltic magma were involved in generation of the precaldera lavas, we also favor an origin for the Amalia Tuff magma that involves protracted AFC of magma that was initially basaltic. The largest shifts in isotope ratios within the crust occur for Sr and Nd because injection of basaltic magma involves large fluxes of mantle-derived Sr and Nd. In contrast, the relatively low Pb content of mantle-derived basaltic magma causes little change in Pb isotopic compositions in either the total or hybridized crust. These effects are directly mirrored in the relatively restricted Nd and Sr (except for very low-Sr units) isotope ratios of the majority of the Latir rocks, in contrast to large variations in Pb isotope ratios. Substantial changes in Sr, Nd, and Pb isotope ratios in the upper mantle can occur during AFC of basaltic magma at the MOHO and subsequent transfer of crustal components to the mantle by crystal accumulation. Although debate on the chemical and isotopic compositions of the lower crust has focussed on granulite-facies metamorphic rocks and the effects of metamorphism on Rb/Sr, Sm/Nd, Th/Pb, and U/Pb ratios and their daugther isotope ratios (e.g., Green et al. 1972; Weaver and Tarney 1980; Ben Othman et al. 1984; McCulloch and Black 1984; Windrim et al. 1984; McCulloch et al. 1987), a substantial volume of the crust beneath large volcanic centers that are younger than the oldest crust in the region may consist of mantle-derived material that equals or exceeds the volume of ancient, granulite-grade crust. In addition, the evidence presented here for extensive injection of mantle-derived basaltic magmas as a driving force for developing large-volume volcanic centers provides a link to recent discussions on the origin of granulite-facies metamorphic rocks that call upon intrusion of mafic magmas as the heat source for metamorphism (e.g., Bohlen and Mezger 1989, and references within).

Acknowledgements. Discussion with K. Foland, J. Hagstrum, J. O'Neil, J. Stacey, and J. Wooden are appreciated, and R. Coleman, G. Mahood, O'Neil, and Wooden are thanked for reviews of an early version of the manuscript. R. Criss and an anonymous reviewer provided helpful journal reviews, and B. Doe provided additional comments. K. Foland is thanked for permitting citation of unpublished $^{40}Ar/^{39}Ar$ ages. R. Fleck provided access to his laboratory where the double-collector mass spectrometry and some of the Rb-Sr chemical separations were done. We are deeply indebted to O'Neil and Wooden who cheerfully provided access to their laboratories, and additional thanks are due Wooden and K. Kyser, who provided some last-minute Pb and O isotope analyses, respectively. J. Banner, G. Hanson, and S. Shirey are thanked for advice during establishment of the REE laboratory at Menlo Park. Material support was provided by the US Geological Survey, fellowships to C.M.J. from the National Science Foundation, State of California, and Stanford University, while C.J.M. was at the U.S.G.S., and N.S.F. grants EAR-861836 and EAR-8803892 while C.M.J. was at the U.W. A portion of the data were obtained in U.S.G.S. and U.W. laboratories while C.M.J. was employed at the University of Wisconsin at Madison, where the manuscript was written. Donna Doskocil and Michelyn Hass assisted in preparation of the manuscript.

References

Axelrod DI, Bailey HP (1976) Tertiary vegetation, climate, and altitude of the Rio Grande depression, New Mexico-Colorado. Paleobiology 2:235–254

Bacon CR (1982) Time-predictable bimodal volcanism in the Coso Range, California. Geology 10:65–69

Ben Othman D, Polve M, Allegre CF (1984) Nd-Sr isotopic composition of granulites and constraints on the evolution of the lower continental crust. Nature 307:510–515

Bigeleisen J, Perlman ML, Prosser HC (1952) Conversion of hydrogenic minerals to hydrogen for isotopic analysis. Anal Chem 24:1356–1357

Bird P (1984) Laramide crustal thickening event in the Rocky Mountain foreland and Great Plains. Tectonics 3:741–758

Bohlen SR, Mezger K (1989) Origin of granulite terranes and the formation of the lowermost continental crust. Science 244:326–329

Borthwick J, Harmon RS (1982) A note regarding ClF_3 as an alternative to BrF_5 for oxygen isotope analysis. Geochim Cosmochim Acta 46:1665–1668

Bottinga Y, Javoy M (1975) Oxygen isotope partitioning among the minerals in igneous and metamorphic rocks. Rev Geophys Space Phys 13:401–418

Cameron KL, Cameron M (1985) Rare earth element, $^{87}Sr/^{86}Sr$, and $^{143}Nd/^{144}Nd$ compositions of Cenozoic orogenic dacites from Baja California, northwestern Mexico, and adjacent west Texas: evidence for the predominance of a subcrustal component. Contrib Mineral Petrol 91:1–11

Campbell IH, Turner JS (1987) A laboratory investigation of assimilation at the top of a basaltic magma chamber. J Geol 95:155–172

Chappell BW, Stephens WE (1988) Origin of infracrustal (I-type) granite magmas. Trans Royal Soc Edinburg: Earth Sci 79:71–86

Chappell BW, White AJR, Wyborn D (1987) The importance of residual material (restite) in granite petrogenesis. J Petrol 28:1111–1138

Christiansen RL, Lipman PW (1972) Cenozoic volcanism and plate-tectonic evolution of the western United States 2. Late Cenozoic. Philos Trans R Soc Lond A271:249–284

Cohen RS, O'Nions RK (1982) The lead, neodymium and strontium isotopic structure of ocean ridge basalts. J Petrol 23:299–324

Cohen RS, Eversen NM, Hamilton PJ, O'Nions RK (1980) U-Pb, Sm-Nd and Rb-Sr systematics of mid-ocean ridge basalt glasses. Nature 283:149–153

Cordell L, Long CL, Jones DW (1986) Geophysical expression of the batholith beneath Questa caldera, New Mexico. J Geophys Res 90:11253–11274

Crisp JA (1984) Rates of magma emplacement and volcanic output. J Volcanol Geotherm Res 20:177–211

Criss RE, Fleck RJ (1987) Petrogenesis, geochronology, and hydrothermal systems of the northern Idaho batholith and adjacent areas based on $^{18}O/^{16}O$, D/H, $^{87}Sr/^{86}Sr$, K-Ar, and $^{40}Ar/^{39}Ar$ studies. US Geol Surv Prof Pap 1436:95–137

Czamanske GK, Dillet B (1988) Alkali amphibole, tetrasilicic mica, and sodic pyroxene in peralkaline siliceous rocks, Questa caldera, New Mexico. Am J Sci 288-A:358–392

DePaolo DJ (1981a) Neodymium isotopes in the Colorado Front

Range and crust-mantle evolution in the Proterozoic. Nature 291:193–196
DePaolo DJ (1981b) Trace-element and isotopic effects of combined wall rock assimilation and fractional crystallization. Earth Planet Sci Lett 53:189–202
Dickin AP, Jones NW (1983) Relative elemental mobility during hydrothermal alteration of a basic sill, Isle of Skye, NW Scotland. Contrib Mineral Petrol 82:147–153
Dickin AP, Exley RA, Smith BM (1980) Isotopic measurement of Sr and O exchange between meteoric-hydrothermal fluid and the Coire Vaigneich granophyre, Isle of Skye, NW Scotland. Earth Planet Sci Lett 51:58–70
Dillet B, Czamanske GK (1987) Aspects of petrology, mineralogy, and geochemistry of the granitic rocks associated with Questa caldera, northern New Mexico. US Geol Surv Open-File Report 87–258, pp 238
Doe BR, Zartman RE (1979) Plumbotectonics, the Phanerozoic. In: Barnes HL (ed) Geochemistry of hydrothermal ore deposits. Wiley, New York, pp 22–70
Doe BR, Lipman PW, Hedge CE, Kurasawa H (1969) Primitive and contaminated basalts from the southern Rocky Mountains, U.S.A. Contrib Mineral Petrol 21:142–156
Druitt TH, Bacon CR (1988) Compositional zonation and cumulus processes in the Mount Mazama magma chamber, Crater Lake, Oregon. Trans R Soc Edinburgh: Earth Sci 79:289–297
Dungan MA, Lindstrom MM, McMillan NJ, Moorbath S, Hoefs J, Haskin LA (1986) Open system magmatic evolution of the Taos Plateau volcanic field, northern New Mexico-I: the petrology and geochemistry of the Servilleta Basalts. J Geophys Res 91:5999–6028
Dupre B, Allegre CJ (1980) Pb-Sr-Nd isotopic correlation and the chemistry of the North Atlantic mantle. Nature 286:17–22
Eaton GP, Christiansen RL, Iyer HM, Mabey DR, Blank HR Jr., Zietz I, Gettings ME (1975) Magma beneath Yellowstone National Park. Science 188:787–796
Farmer GL, DePaolo DJ (1987) Nd and Sr isotope study of hydrothermally altered granite at San Manuel, Arizona: implications for element migration paths during the formation of porphyry copper ore deposits. Econ Geol 84:1142–1151
Gray CM, Oversby VM (1972) The behavior of lead isotopes during granulite facies metamorphism. Geochim Cosmochim Acta 36:939–952
Gregory RT, Criss RE (1986) Isotopic exchange in open and closed systems. In: Valley JW, Taylor HP Jr., O'Neil JR (eds) Reviews in mineralogy 16: Stable isotopes in high temperature geological processes. Mineral Soc Am, Washington DC, pp 91–127
Green TH, Brunfelt AO, Heier KS (1972) Rare-earth element distribution and K/Rb ratios in granulites, mangerites and anorthosites, Lofoten-Vesteraalen, Norway. Geochem Cosmochim Acta 36:241–257
Grove TL, Kinzler RJ, Baker MB, Donnelly-Nolan JM, Lesher CE (1988) Assimilation of granite by basaltic magma at Burnt Lava flow, Medicine Lake volcano, northern California: decoupling of heat and mass transfer. Contrib Mineral Petrol 99:320–343
Hagstrum JT, Johnson CM (1986) A paleomagnetic and stable isotope study of the pluton at Rio Hondo near Questa, New Mexico: implications for C.R.M. related to hydrothermal alteration. Earth Planet Sci Lett 78:296–314
Hagstrum JT, Lipman PW (1986) Paleomagnetism of the structurally deformed Latir volcanic field, northern New Mexico: relations to formation of the Questa caldera and development of the Rio Grande rift. J Geophys Res 91:7383–7402
Halliday AN, Hildreth W, Christiansen R, MacLaren F (1986) Fine resolution of crustal contamination in the Yellowstone Plateau volcanic field. Terra Cognita 6:198–199
Hegner E, Unruh D, Tatsumoto M (1986) Nd-Sr-Pb isotope constraints on the sources of West Maui volcano, Hawaii. Nature 319:478–480
Helz RT (1976) Phase relations of basalts in their melting ranges at $PH_2O = 5$ kb. Part II, melt compositons. J Petrol 17:139–193
Henderson P (1982) Inorganic geochemistry. Pergamon, Oxford, pp 353
Hildreth W (1981) Gradients in silicic magma chambers: implications for lithospheric magmatism. J Geophys Res 86:10153–10192
Hildreth W, Moorbath S (1988) Crustal contributions to arc magmatism in the Andes of Central Chile. Contrib Mineral Petrol 98:455–489
Jacobsen SB, Wasserburg GJ (1980) Sm-Nd isotopic evolution of chondrites. Earth Planet Sci Lett 50:139–155
Jagoutz E, Palme H, Baddenhausen H, Blum K, Cendales M, Dreibus G, Spettel B, Lorenz V, Wänke H (1979) The abundances of major, minor and trace elements in the earth's mantle as derived from primitive ultramafic nodules. Proc Tenth Lunar Planet Sci Conf, 2031–2050
Johnson CM (1989) Isotopic zonations in silicic magma chambers. Geology (in press)
Johnson CM, Lipman PW (1988) Origin of metaluminous and alkaline volcanic rocks of the Latir volcanic field, northern Rio Grande rift, New Mexico. Contrib Mineral Petrol 100:107–128
Johnson CM, O'Neil JR (1984) Triple junction magmatism: a geochemical study of Neogene volcanic rocks in western California. Earth Planet Sci Lett 71:241–262
Johnson CM, Czamanske GK, Lipman PW (1989) Geochemistry of intrusive rocks associated with the Latir volcanic field, New Mexico, and contrasts between evolution of plutonic and volcanic rocks. Contrib Mineral Petrol 103:90–109
Kelley SA, Duncan IJ (1986) Late Cretaceous to middle Tertiary tectonic history of the northern Rio Grande rift. J Geophys Res 91:6246–6262
Larson PB, Taylor HP Jr (1986) $^{18}O/^{16}O$ ratios in ash-flow tuffs and lavas from the central Nevada caldera complex and the central San Juan caldera complex, Colorado. Contrib Mineral Petrol 92:146–156
Laughlin AW, Rehrig WA, Mauger RL (1969) K-Ar chronology and sulphur and strontium isotope ratios at the Questa mine, New Mexico. Econ Geol 64:903–909
Leonardson RW, Dunlap G, Starquist VL, Bratton GP, Meyer JW, Osborn LW, Atkin SA, Molling PA, Moore RF, Olmore SD (1983) Preliminary geology and molybdenum deposits at Questa, New Mexico. In: The genesis of Rocky Mountain ore deposits: changes with time and tectonics. Proc Denver Region Explor Geol Soc Symp, pp 151–155
Lipman PW (1983) The Miocene Questa caldera, northern New Mexico: relation to batholith emplacement and associated molybdenum mineralization. In: The genesis of Rocky Mountain ore deposits: changes with time and tectonics. Proc Denver Region Explor Geol Soc Symp, pp 133–147
Lipman PW (1984) The roots of ash flow calderas in western North America: windows into the tops of granitic batholiths. J Geophys Res 89:8801–8841
Lipman PW (1988) Evolution of silicic magma in the upper crust: the mid-Tertiary Latir volcanic field and its cogenitic granitic batholith, northern New Mexico, USA. Trans R Soc Edinburgh: Earth Sci 79:265–288
Lipman PW, Reed JC Jr (1989) Geologic map of the Latir volcanic field and adjacent areas, northern New Mexico. US Geol Surv Misc Map I-1907
Lipman PW, Doe BR, Hedge CE, Steven TA (1978) Petrologic evolution of the San Juan volcanic field, southwestern Colorado: Pb and Sr isotope evidence. Geol Soc Am Bull 89:59–82
Lipman PW, Mehnert HH, Naeser CW (1986) Evolution of the Latir volcanic field, northern New Mexico and its relation to the Rio Grande rift, as indicated by K-Ar and fission-track dating. J Geophys Res 91:6329–6346
Loeffler BM, Futa K (1985) Sr and Nd isotope systematics of the Jemez volcanic field. EOS Am Geophys Union 46:1110
Ludington S (1981) Quartz-pyrite-molybdenite stockwork near South Fork Peak, Taos County, New Mexico. US Geol Surv Open-File Rep 81–180, pp 8

Macdonald R, Smith RL (1988) Relationships between silicic plutonism and volcanism: geochemical evidence. Trans R Soc Edinburgh: Earth Sci 79:257–263

Mahood GA, Halliday AN (1988) Generation of high-silica rhyolite: a Nd, Sr, and O isotopic study of Sierra La Primarera, Mexican Neovolcanic Belt. Contrib Mineral Petrol 100:183–191

McCulloch MT, Black LP (1984) Sm-Nd isotopic systematics of Enderby Land granulites and evidence for the redistribution of Sm and Nd during metamorphism. Earth Planet Sci Lett 71:46–58

McCulloch MT, Bradshaw JY, Taylor SR (1987) Sm-Nd and Rb-Sr isotopic and geochemical systematics in Phanerozoic granulites from Fiordland, Southwest New Zealand. Contrib Mineral Petrol 97:183–195

Musselwhite DS, DePaolo DJ, McCurry M (1989) The evolution of a silicic magma system: isotopic and chemical evidence from the Woods Mountains volcanic center, eastern California. Contrib Mineral Petrol 101:19–29

Nelson BK, DePaolo DJ (1984) 1,700-Myr greenstone volcanic successions in southwestern North America and isotopic evolution of Proterozoic mantle. Nature 312:143–146

Nelson BK, DePaolo DJ (1985) Rapid production of continental crust 1.7 to 1.9 b.y. ago: Nd isotopic evidence from the basement of the North American mid-continent. Geol Soc Am Bull 96:746–754

Nicholls IA, Harris KL (1980) Experimental rare earth element partition coefficients for garnet, clinopyroxene and amphibole coexisting with andesite and basaltic liquids. Geochim Cosmochim Acta 44:287–308

Novak SW (1985) Geology and geochemical evolution of the Kane Springs Wash volcanic center, Lincoln County, Nevada. Unpubl. PhD thesis, Stanford University, pp 173

Patchett PJ, Ruiz J (1987) Nd isotopic ages of crust formation and metamorphism in the Precambrian of eastern and southern Mexico. Contrib Mineral Petrol 96:523–528

Perry FV, DePaolo DJ, Baldridge WS (1983) Nd and Sr isotope evidence for the origin of Mount Taylor lavas and depleted mantle beneath the Colorado Plateau-Rio Grande rift, central New Mexico. EOS Am Geophy Union 64:753

Perry FV, Baldridge WS, DePaolo DJ (1987) Role of asthenosphere and lithosphere in the genesis of Cenozoic basaltic rocks from the Rio Grande rift and adjacent regions of the southwestern United States. J Geophys Res 92:9193–9213

Phelps DW, Gust DA, Wooden JL (1983) Petrogenesis of the mafic feldspathoidal lavas of the Raton-Clayton volcanic field, New Mexico. Contrib Mineral Petrol 84:182–190

Prodehl C, Lipman PW (1989) Crustal structure of the Rocky Mountain region. In: Pakiser LC, Mooney WD (eds) Geophysical framework of the continental United States. Geol Soc Am Mem, in press

Reed JC Jr (1984) Proterozoic rocks of the Taos Range, Sangre de Cristo Mountains, New Mexico. 35th Field Conf New Mexico Geol Soc, pp 179–185

Shaw HR (1985) Links between magma-tectonic rate balances, plutonism, and volcanism. J Geophys Res 90:11275–11288

Sheppard SMF (1986) Characterization and isotopic variations in natural waters. In: Valley JW, Taylor HP Jr, O'Neil JR (eds) Reviews in mineralogy 16: Stable isotopes in high temperature geological processes. Mineral Soc Am, Washington DC, pp 165–183

Smith RL (1979) Ash flow magmatism. Geol Soc Am Spec Pap 180:5–27

Sparks RSJ, Marshall LA (1986) Thermal and mechanical constraints on mixing between mafic and silicic magmas. J Volcanol Geotherm Res 29:99–124

Spera F (1980) Thermal evolution of plutons: a parameterized approach. Science 207:299–301

Spera FJ, Crisp JA (1981) Eruption volume, periodicity, and caldera area: relationships and inferences on development of compositional zonation in silicic magma chambers. J Volcanol Geotherm Res 11:169–187

Stacey JS, Hedlund DC (1983) Lead-isotopic compositions of diverse igneous rocks and ore deposits from southwestern New Mexico and their implications for early Proterozoic crustal evolution in the western United States. Geol Soc Am Bull 94:43–57

Stacey JS, Kramers JD (1975) Approximation of terrestrial lead isotope evolution by a two-stage model. Earth Planet Sci Lett 26:207–221

Staudigel H, Zindler A, Hart SR, Leslie T, Chen C-Y, Clauge D (1984) The isotope systematics of a juvenile intraplate volcano: Pb, Nd, and Sr isotope ratios of basalts from Loihi Seamount, Hawaii. Earth Planet Sci Lett 69:13–29

Steven TA (1975) Middle Tertiary volcanic field in the southern Rocky Mountains. Geol Soc Am Mem 144, pp 75–94

Stille P, Unruh DM, Tatsumoto M (1983) Pb, Sr, Nd and Hf isotopic evidence of multiple sources for Oahu, Hawaii basalts. Nature 304:25–29

Suzuoki T, Epstein S (1976) Hydrogen isotope fractionation between OH-bearing minerals and water. Geochim Cosmochim Acta 40:1229–1240

Taylor HP Jr (1968) The oxygen isotope geochemistry of igneous rocks. Contrib Mineral Petrol 19:1–71

Taylor HP Jr (1977) Water/rock interactions and the origin of H_2O in granitic batholiths. J Geol Soc Lond 133:509–558

Taylor HP Jr (1980) The effects of assimilation of country rocks by magmas on $^{18}O/^{16}O$ and $^{87}Sr/^{86}Sr$ systematics in igneous rocks. Earth Planet Sci Lett 47:243–254

Tegtmeyer K, Farmer GL (1987) Nd isotopic evidence for the origin of late Tertiary metaluminous and peralkaline rhyolite in the Great Basin. EOS Am Geophys Union 68:1512

Thompson RA, Machette MN (1989) Geologic map of the San Luis Hills area, Conejos and Costilla counties. Colorado. US Geol Surv Miscl Invest Map I-1906

Thompson RA, Dungan MA, Lipman PW (1986) Multiple differentiation processes in early-rift calc-alkaline volcanics, northern Rio Grande rift, New Mexico. J Geophys Res 91:6046–6058

Verma SP (1983) Magma genesis and chamber processes at Los Humeros caldera, Mexico – Nd and Sr isotope data. Nature 302:52–55

Verma SP (1984) Sr and Nd isotopic evidence for petrogenesis of mid-Tertiary felsic volcanism in the mineral district of Zacatecas, Zac. (Sierra Madre Occidental), Mexico. Iso Geosci 2:37–53

Wasserburg GJ, Jacobsen SB, DePaolo DJ, McCulloch MT, Wen T (1981) Precise determination of Sm/Nd ratios, Sm and Nd isotopic abundances in standard solutions. Geochim Cosmochim Acta 45:2311–2332

Weaver BL, Tarney J (1980) Rare earth geochemistry of Lewisian granulite-facies gneisses, northwest Scotland: implications for the petrogenesis of the Archean lower continental crust. Earth Planet Sci Lett 51:279–296

Williams S (1984) Late Cenozoic volcanism in the Rio Grande rift: trace element, strontium isotopic and neodymium isotopic geochemistry of the Taos Plateau volcanics. Unpubl. PhD thesis, University of Minnesota, Minneapolis, pp 211

Windrim DP, McCulloch MT, Chappell BW, Cameron WE (1984) Nd isotopic systematics and chemistry of Central Australian sapphirine granulites: an example of rare earth element mobility. Earth Planet Sci Lett 70:27–39

Zartman RE, Doe BR (1981) Plumbotectonics – the model. Tectonophys 75:135–162

Received December 16, 1988 / Accepted July 20, 1989
Editional responsibility: T. Grove